Renewable and Sustainable Energy Reviews 15 (2011) 4855–4875

Contents lists available at SciVerse ScienceDirect

Renewable and Sustainable Energy Reviews

journal homepage: www.elsevier.com/locate/rser

Compact heat exchangers: A review and future applications for a new generation of high temperature solar receivers

Qi Li [a,b,*], Gilles Flamant [b], Xigang Yuan [a], Pierre Neveu [b,c], Lingai Luo [d]

[a] State Key Laboratory of Chemical Engineering, Tianjin University, 300072 Tianjin, China
[b] Processes, Materials and Solar Energy laboratory (CNRS-PROMES), 66120 Odeillo Font-Romeu, France
[c] University of Perpignan, (UPVD) Tecnosud, 66100 Perpignan, France
[d] Laboratoire Optimisation de la Conception et Ingénierie de l'Environnement (LOCIE), Université de Savoie, Campus Scientifique, Savoie Technolac, 73376 Le Bourget-du-Lac cedex, France

ARTICLE INFO

Article history:
Received 26 January 2011
Accepted 7 July 2011
Available online 15 September 2011

Keywords:
Compact heat exchanger
Solar receiver
Heat transfer enhancement

ABSTRACT

This paper gives a review on performances of compact heat exchangers (CHEs), including well-established devices, some relative newcomers to the market and also designs still being tested in the laboratory. The structures of the CHEs are briefly introduced, and their heat transfer enhancement mechanisms, as well as their advantages and limitations, are summarized. Then, different heat transfer enhancement technologies in CHEs are compared and their thermo-hydraulic performances are analyzed on the basis of available correlations for heat transfer and friction factor developed by various investigators quoted in the open literature. Finally, the technologies that may fit the specifications for a new generation of solar receiver, which is a critical component of the Concentrated Solar Power (CSP) system, are proposed. It is concluded, among others in the review, that solar receivers based upon CHE technology have been rarely reported, and therefore, more work is needed in this field for a comprehensive understanding and to improve the uses of new energy sources and contribute to sustainability.

Contents

* Corresponding author at: State Key Laboratory of Chemical Engineering, Tianjin University, 300072 Tianjin, China. Fax: +86 22 27404496.
E-mail address: qili@tju.edu.cn (Q. Li).

1364-0321/$ – see front matter © 2011 Elsevier Ltd. All rights reserved.
doi:10.1016/j.rser.2011.07.066

1. Introduction

Efficient design of solar receivers is critical for the Concentrated Solar Power (CSP) system. Advanced CSP system uses pressurized gas solar receiver associated with a Brayton cycle [1,2]. In this case, the working fluid of the gas solar receiver and of the electric generator is the same. Pressurized air is usually selected as the working fluid considering the cost and environmental impacts. In an open cycle the air heated to high temperature inside the solar receiver, flows directly through the turbine or via a combustion chamber (fossil fuel back-up) where it is expanded. Closed cycles have been envisioned using supercritical carbon dioxide as working fluid [3]. Both options require the use of heat exchange device having superior performance and reliable mechanical characteristics at high pressure and high temperature to guarantee the cycle efficiency, moreover geometric constraints are also important for such application. Thus, compact heat exchangers (CHEs) technologies are expected to be one of the solutions for this new generation of solar receiver.

This paper reviews various technologies of CHE used in industry or still being tested in the laboratory to provide useful insights into the design of solar receiver. Their structures and heat transfer enhancement mechanisms are briefly introduced. Then, a selection of potential CHEs technologies is proposed for the new generation of solar receiver accounting for the specific constraints of such systems, in particular the surface to volume heat transfer.

2. Types of compact heat exchangers

CHEs are characterized by having a comparatively large area density. Area density is the ratio of heat transfer surface to heat exchanger volume. Their large area density, indicating small hydraulic diameter for fluid flow, results in a higher efficiency than conventional shell-and-tube heat exchanger in a significantly smaller volume. A CHE has been arbitrarily defined by Shah [4,5] as having an area density over 700 m^2/m^3 or a hydraulic diameter $D_h \leq 6$ mm if at least one fluid is gas, and in excess of 400 m^2/m^3 when operating in liquid or multi-phase streams. A typical shell-and-tube heat exchanger has an area density of less than 100 m^2/m^3 on one fluid side with plain tubes, and 2–3 times greater than that with high-fin-density low-finned tubing [6]. Human lungs are one of the most compact heat exchangers, having an area density of about 17,500 m^2/m^3, which is equivalent to 0.19 mm diameter tubes. Some micro-scale heat exchangers under development, having an area density greater than about 15,000 m^2/m^3 or 1 $\mu m \leq D_h \leq 100$ μm, are as compact as the human lung and even more compact [4–7].

As easily understandable, small flow passages have two effects, a tendency to laminar flow in the channels and a high pressure drop. Laminar flow is associated with low heat transfer coefficients, and therefore, the efficiency is necessarily improved by various heat transfer enhancement techniques, which have brought in a variety of CHEs. Some types of CHEs have been in routine use for many decades. Others have recently been introduced into the market, while a number of types are still being tested in the laboratory.

The necessary reduction of energy consumption, capital investment minimization and improvement of adaptability of components has led to rapid development of the research on CHEs and their applications in many areas such as aerospace, automobile, gas turbine power plant, nuclear reaction, and some others, especially in high temperature services.

2.1. Plate heat exchanger (PHE)

The first patent for a PHE was granted to a German, Albretch Dracke in 1878 and the first commercially operational PHE was invented in 1923 by Dr. Richard Seligman, the founder of the Aluminium Plant and Vessel Company Ltd. (APV) in England [8]. The traditional concept of a PHE is the plate-and-frame heat exchanger (Fig. 1). It consists of a series of corrugated plates supported by a rigid frame. The corrugations on adjacent plates contact or cross each other forming highly interrupted and tortuous channels. Sealing between streams is accomplished by gaskets. In addition, multi-pass can be accommodated by blanking plates within the stack. Various specifications can be matched by adding or removing some plates or with different plate patterns.



Fig. 1. AlfaRex™ plate heat exchanger (courtesy of Alfa Laval).

It is believed that heat transfer coefficients are high in PHEs due to small hydraulic diameter and strong interaction between the flow inside the channel and over the corrugation crest, accompanied by the secondary flows [9,10], as (1) they increase turbulence and advection of fluid from the center of the channel to the near-wall region; (2) they are responsible for the breakup and separation of the boundary layer and its new formation and reattachment [11]; (3) they decrease the probability of appearance of stagnation areas and fouling to 10–25% of that of a shell-and-tube heat exchanger [6].

Many works have been done to obtain a better understanding about the heat transfer characteristics and related flow mechanisms of the PHEs, including flow visualization by Focke and Knibbe [12], Herman and Mayinger [13–15], Paras et al. [16,17], Sang et al. [18], Dovic et al. [10], Asano et al. [19], Li et al. [20]; heat transfer and pressure drop measurement by Rao et al. [21,22], Durmus et al. [23], Jeong et al. [24], Elshafei et al. [11]; and also numerical simulation by Fernandes et al. [25–28], Kanaris et al. [17,29,30], Tsai et al. [31].

The correlations for the prediction of thermal and hydraulic performances of PHEs are available in literature based on experimental data [23,32,33] with neural network method [34], physically based mathematical model [10], or numerical simulation [30] to provide simplicity in analysis of PHEs and help to heat exchanger designer and manufacturer. Ayub [35] summarized over thirty single-phase heat transfer and pressure drop correlations for PHEs.

The main weakness is that the plate-and-frame heat exchangers are restricted to low or moderate temperature and pressure applications due to the use of gaskets. Beside this, for equivalent flow velocities, pressure drop in a PHE is relatively high due to its narrow passages which can be blocked by particulate contaminants in the fluid, and ineffective transversely vortices and zigzag flow patterns [12,36]. Although the traditional plate-and-frame heat exchanger is still the most often used in industries, its disadvantages tricked many efforts, which resulted in variant models of PHEs. The evolution can be either structure construction or plate pattern [37].

In the 1990s, Alfa Laval developed the wide-gap PHEs with no metal to metal contact between adjacent plates for fluids containing fibers or coarse particles as well as highly viscous fluids [38]. The double-wall PHE was first introduced in 1986 by Dahlgren et al. [39] for uses when mixing of the fluids must be avoided due to possible contamination or to an undesirable reaction. It substitutes the single plates with pairs of identical ones. Should a failure occur, the leak will enter the gap between them, and then is conveyed to atmosphere, ensuing that leak will be clearly visible outside the heat exchanger.

For high pressure and high temperature applications or where a more compact PHE is required, brazing or laser welding is generally used instead of gaskets. Advances in brazing and welding technology have made the gasket-free PHEs like brazed, semi-welded and all-welded PHEs increasingly practical. In the last two decades, Compabloc^{TM} fully-welded PHE from Vicarb (now Alfa Laval) [40] has been proven to be high-performance and cost-effective for duties with temperature cross or close temperature approaches. It consists of welded plates covered on all sides by panels as a pressure vessel, producing cross-flow channels with overall co-current or counter-current operation. The unit can be easily dismantled for cleaning and inspection. And multi-pass configuration is available by the use of baffles.

The patented Maxchanger® all-welded PHE from Tranter [41] offers high performance for clear liquid, small-volume flows at high pressure. Dimpled plates are arranged alternately and welded together at the sides to form fluid channels. Spacers isolate the channels and induce countercurrent flow. The numerous dimples provide maximum pressure resistance and heat transfer.

The driving force behind the development of welded PHEs was the desire to combine superior thermal and hydraulic performances and great compactness of PHEs with high mechanical integrity under high temperature and high pressure of shell-and-tube designs. Based on such concept, three novel designs were recently introduced in the market.

One is generally categorized as Shell and Plate heat exchanger [42,43]. A pairs of round plates are fabricated into a cassette by welding in the port hole. These cassettes are perimeter welded together, producing an accordion-like core, and then housed within a cylindrical pressure vessel which creates a second flow path—the 'Shell flow side'.

Different from the Shell and Plate heat exchanger, APV hybrid all-welded PHE [40] is integrate with shell-and-tube heat exchanger's 'tube flow' and gasket PHE's plate flow. Pairs of plates are welded back to back forming the elliptical tube channels on the tube flow side and parallel wave flow passage on the plate flow side. The plate side flow and the tube side flow are arranged in cross flow configuration in one or multiple passes over the plates.

The other is Alfa Laval Packinox all-welded PHE [44], which is a stack of plates placed within a pressure vessel pressurized with the recycling gas. All heat transfer takes place within the stack so that no process fluids circulate inside the pressure vessel. The plates are exposed only to the differential pressure of the fluids. The pressure vessel is used to withstand the operating pressure and protect the bundle. The heat exchanger operates in true counter-counter flow with an exceptional degree of safety for both plant personnel and the environment, even in high-pressure applications.

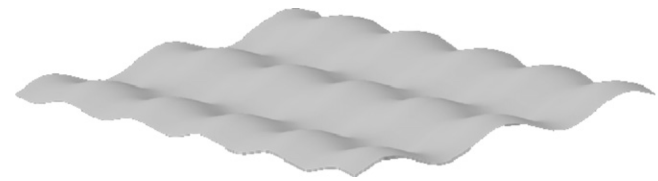


Fig. 2. Plate with longitudinal and transverse corrugations.

The thermal and hydraulic performances of PHEs are strongly influenced by the plate surface corrugation patterns. Many different surface types have been developed.

Plates with corrugations perpendicular to the flow direction are known as washboard plates, while those with corrugations at an angle are known as chevron plates. The chevron plates with a sinusoidal shape have generally been the most successful design offered by the majority of PHE manufacturers [9]. The washboard type provides a wider gap, fewer contact points and requires thicker and more costly material compared to chevron plates. When the gap between the plates lies at the range of 6–7 mm, wide-gap chevron plates often replace the traditional washboard plates to achieve greater mechanical strength with reduced plate thickness.

The chevron type corrugations are characterized by the angle of the corrugations to the flow direction. An obtuse arrow angle means a large thermal driving force, high thermal performance and high pressure drop. Plates with high and low chevron angles can be used within a single PHE. A novel extension of this approach is a single mixed chevron plate [8] like Tranter's Ultraflex plate, whose surface is partitioned into four or more segments, with each having a different chevron angle corrugation to match better the pressure drop and heat transfer constraints, optimize the surface area at minimum pumping power, and for unequal flow rates.

Corrugated plate patterns cause high turbulence so that the overall heat transfer coefficient is 3–5 times greater than a shell-and-tube heat exchanger. Heat transfer coefficient can be equal to the values for tubes in which the Reynolds numbers are 5 times higher, and 3–4 times higher than that for smooth channels can be achieved [45].

Bojesen [46] modified chevron plates with a series of dents, indents, recesses, protrusions and/or additional corrugations outside the plate contact points, increasing the NTU-VALUE more than 5%. Rausing [47] presented a plate comprising a number of turbulent-promoting protrusions (spherical, ellipsoid, waves or grooves). The protrusions have a surface profile for promoting breakup of laminar boundary layers. Asterisk type plates are studied by Durmus et al. [23]. Jeong et al. [24] investigated chevron elliptic and round embossing plates. It is found that the elliptic embossing type gives better heat transfer performance than the chevron type and a lower pressure drop than the other plates under the same geometric and thermal conditions.

A new-type corrugation [48] was designed consisting of longitudinal and transverse corrugations (Fig. 2). The compound corrugation surface can be formed if the longitudinal curve is scanning in the path of the transverse one. The flow resistance in this PHE, compared with the traditional chevron type, was decreased by more than 50%, and heat transfer performance was decreased by about 25%.

Li et al. [20] found that the inclined discrete rib plates can enhanced heat transfer by 20–25% at the same pumping power compared with the commonly used inclined continuous rib plates. Multiple longitudinal vortices are generated by the inclined cross discrete rib pair, namely the front vortex, the rear vortex and the main vortex. Longitudinal vortex is an effective flow pattern for

heat transfer enhancement at relatively lower pressure drop from the point of the field synergy principle proposed by Guo [49,50].

Because there are many different types of PHE and numerous manufactures, it is difficult to precisely summarize the operating limits. The purpose here is to give a general overview; a summary of typical operating ranges for PHEs is given in Table 1. This is based on the products from the following manufactures: Alfa Laval, Tranter, APV and GEA. In most of the cases, the maximum pressure and temperature cannot be reached simultaneously.

The area density of PHE ranges from 120 to 660 m^2/m^3 [6]. The hydraulic diameter lies between 2 and 10 mm for most plates. Typically, the number of plates is between 10 and 100, which gives 5–50 channels per fluid [51].

One advantage of the PHEs is the greatly reduced space requirements. The surface area required for a PHE is 30–50% that of a shell-and-tube heat exchanger for a given heat duty, thus in turn reducing the cost. For the same effective heat transfer area, the weight and volume of PHEs are approximately only 30% and 20%, respectively, of those of shell-and-tube heat exchangers [8]. They can have 50% less volume than a fined tube heat exchanger, and 60% less than a serpentine one for the same thermal performance [52].

Choice of gasket materials is critical to the reliable operation of PHEs [53]. Gaskets are generally made from a variety of elastic and formable materials, such as rubber and its different polymerized forms [8]. The gasket materials restrict the use of PHEs in highly corrosive applications and also limit the maximum operating temperature to avoid the use of expensive gasket materials.

The thermal conductivity of the plate is an important consideration for the thermal–hydraulic design of a PHE. Therefore, plate materials with higher thermal conductivity are preferred. A wide variety of plate materials are available: Stainless steel (types 304, 316, 317, 304L, 316L, 317Ti), Alloy AL6XN, Alloy 904L, Alloy 27-7MO, Alloy 254 SMO; Nickel 200, Alloy G-30, Alloy B-2, Alloy C-22, Alloy C-276, Alloy C-2000, Alloy 33; Titanium (Gr. 1), Titanium palladium (Gr. 7&11), tantalum.

Stainless steel is a most commonly used metal for the plates because of its ability to withstand high temperature, its strength, and its corrosion resistance [8,23]. The Alfa Laval Diabon graphite PHE and polymer plates are developed for highly corrosive fluids.

2.2. Plate-fin heat exchanger (PFHE)

PFHEs have been produced since the 1910s in the auto industry (copper fin-brass tubes), since the 1940s in the aerospace industry and for liquefaction of natural gases since the 1950s using aluminium because of the better mechanical characteristics of aluminium at low temperatures [6].

PFHE is a form of CHE consisting of a block of alternating layers of corrugated sheets (fins), separated by parting sheets and enclosed at the edges by side bars to create a series of finned chambers (Fig. 3). The fins and the parting sheets are assembled by brazing in a vacuum furnace to become a single rigid core. The heat exchanger can be made of one or more cores. The number of the plate and the fin layer, the size of the plate and fin, the height of the fin and the type of fin are engineered for optimum performance [51,54].

In a PFHE, the fins are easily able to be rearranged. This allows the PFHE to operate in cross-flow, counter-flow, cross-counterflow or co-current flow. A simple cross-flow layout is generally suitable and used extensively for low or moderate duties, and is especially effective when one side is a low pressure gas. For heavier duty tasks, the counter-flow pattern frequently offers an efficient solution. The higher levels of efficiency achieved by counter-flow units are essential to most low temperature applications.

Heat is transferred from hot fluid through the fin interface to the separator plate and through the next set of fins into the adjacent cold fluid. The plate and the fin base directly brazed to the plate, which make up the primary heat transfer surface, separate the two or more fluids, and the fins form the individual flow passages. The fins have two functions, firstly to act as the secondary (or indirect, extended) heat transfer surface to increase the effective heat transfer surface area, obtain a low hydraulic diameter, reduce the thermal resistance and increase the total heat transfer from the surface for the same temperature difference, and secondly to withstand the design pressure at the design temperature as a structural component. Various types of fin geometry are therefore developed to meet both requirements depending on the application. Table 2 provides general information on common application for each type of fin.

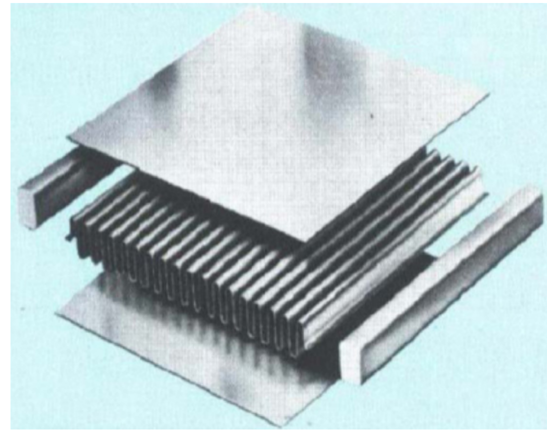


Fig. 3. PFHE layer illustration of main components (courtesy of Chart).

The enhancement in heat transfer achieved with plain fins is mainly due to the increased area density, rather than any increase in the heat transfer coefficient. While wavy and corrugated channels herringbone fins both enhance heat transfer by promoting mixing due to generated complex secondary flows and boundary layer separation. The serrated and perforated fins are also categorized as interrupted fins. Surface interruption enhances heat transfer through two independent mechanisms [56]. First, surface interruption prevents the continuous growth of the thermal boundary layer by periodically interrupting it. Thus the thicker thermal boundary layer in continuous fins, which offers higher thermal resistance to heat transfer, is maintained thin and the resistance to heat transfer is reduced. This heat transfer enhancement mechanism occurs even at low Reynolds numbers when the flow is steady and laminar. Above a critical Reynolds number, the interrupted surfaces offer an additional mechanism of heat transfer enhancement by inducing self-sustained oscillations in the flow in the form of shed vortices. Vortices roll up near the leading edge of the fins and subsequently travel downstream along the fin surface. Von Karman vortices are also observed to form at the trailing edge of the fins and travel downstream in the wake before encountering the next fin element. They act as large scale mixers and continuously bring in fresh fluid from the free-stream on their downstream side towards the fin surface [57,58] and eject the fluid on their upstream side away from the fin surface. There is, of course, an associated increase in the pressure drop and thus pumping power. This is partly due to the higher skin friction associated with the hydrodynamic boundary layer restarting. In addition, in the unsteady flow regime, the time-dependent flow behavior associated with vortex shedding increases frictional loss through the Stokes layer dissipation and form drag through Reynolds stresses [59]. The two independent mechanisms simultaneously influence both the overall heat transfer and the pumping power requirement. Therefore, design optimization must take into account the impact of design parameters on the relative importance

Table 1
Typical operating ranges for PHEs.

Types of PHE	Plate patterns	Operating temperature (°C)	Maximum pressure (bar)	Flow rate (m^3/h)	Heat transfer area (m^2)	Main products in the market
Gasketed conventional	Herringbone Zigzag	Rubber: −35 to 200 Graphite: −20 to 250	35	0–5768	0.1–3800/unit 0.02–5/plate	GEA-Ecoflex APV-ParaFlow Tranter-Superchanger-GC & GL
Wide-gap	Washboard Wide-Gap	−35 to 200	16	2000	1472.5/unit 0.28–1.56/plate	GEA-Ecoflex-Free Flow Tranter-Superchanger-GF APV-Easy flow
Double-wall	Herringbone Zigzag	−35 to 200	16	200	400/unit	Alfa Laval Tranter-GD GEA-Safetytherm APV-Duo Safety
Brazed	Herringbone	−195 to 225	45	160	75/unit	APV Alfa Laval GEA-EcoBraze
Semi-welded	Herringbone Zigzag	−45 to 220	40	970	2500/unit 0.16–1.82/plate	APV-Paraweld Alfa Laval Tranter GEA-EcoFlex-LWC
AlfaRex	Herringbone	−50 to 350	40	700	250/unit 2.056–8.4/plate	Alfa Laval
Maxchanger	Dimpled	−195 to 540 (538[a])	115	15	4/unit	Tranter
Compabloc	Herringbone Dimpled	−195.5 to 350 (170[a])	45	4000	0.7–840/unit 0.061–0.989/plate	Tranter-Ultramax GEA-Ecoweld-Bloc Alfa Laval-Compabloc
Hybrid	Hybrid	−200 to 900	80	-	6–8000/unit	GEA-Ecoweld-Flex APV-Hybrid
Shell & Plate	Herringbone	−200 to 950(230[a])	200	1000	0.025–1.55/plate	Alfa Laval-Disc Tranter-Supermax GEA-EcoWeld-Shell Vahterus APV-Parashell
Packinox	Herringbone	550	120 (40[b])	–	1000–20,000/unit	Alfa Laval

[a] Maximum differential temperature.
[b] Maximum differential pressure.

of the different heat transfer enhancement mechanisms and their attendant effect on pumping power.

Vortex generators are often categorized as a type of fin because they are generally mounted on the primary heat transfer surface like other types of fin. However, they do not significantly change the effective heat transfer surface area of the plate, but they increase the heat transfer coefficient by creating longitudinally spiraling vortices which promote mixing between the wall and core regions of the flow. Brockmeier et al. [60] studied five configurations of fin, and their results show that the vortex generator surface provides the largest reduction in heat exchanger surface area, and thus, the largest reduction in heat exchanger volume for fixed hydraulic diameter, pumping power, heat duty, and mass flow rate. It is followed by the offset strip fin and louvered fin surfaces. The two surfaces are fairly close to each other. These surfaces all significantly reduce the required heat transfer area compared to the rectangular plain fin surface. The triangular plain fin surface is shown to be the least effective.

A review [61] on the research and developments of offset and wavy compact plate-fin heat exchangers has been carried out. The information obtained is divided into three parts: offset fins, wavy fins and non-uniformity of inlet fluid flow. This review helps the

Table 2
Common application of each type of fin [55].

Corrugation	Description	Application	Features	
			Relative pressure drop	Relative heat transfer
Plain	Straight, triangular or rectangular	For general use	Lowest	Lowest
Perforated	Straight, with small holes	Most frequently used for any purpose	low	low
Serrated	Straight, offset half a pitch—usually about every 3–4 mm	Frequently used, especially for low pressure gas streams in air separation plants	Highest	highest
Herringbone or long-lanced serrated	Smooth but in waves of about 10 mm pitch to provide a zigzag path, or serrated with long serration pitch	Often used for gas streams with low allowable pressure drop	High	high

researchers to carry out their further research in this field and also gives awareness for the designers to select the accurate design data (f and j) for the optimum design (i.e., minimum pumping power and efficient heat transfer) of compact heat exchangers. This optimum design in turn leads to energy savings in terms of cost.

An artificial neural network (ANNs) based on back propagation algorithm has been developed to predict the thermal performance of PFHEs [62].

The secondary flow is observed with its axis parallel to the main flow. The churning of the fluid is found to enhance the mean temperature of the fluid significantly. A compactness of the exchanger up to 19.92% is achievable by using a rectangular wing with a 26° angle of attack. The stamped wings are easy to produce on the inclined surfaces of the triangular fins and the combined spanwise Nusselt number for the stamped wing at an attack angle of 20° and the Reynolds number 100 is 12.74% higher as compared to a plate-fin without any vortex generator [63]. The results show that the delta wing vortex generator increases the heat transfer performance of the heat exchanger. Heat transfer increases with the increase in the angle of attack and with the Reynolds number. There is a simultaneous increase in the pumping power required, which further increases with higher angles of attack but decreases with an increase in the Reynolds number. Stamped delta wing is slightly less efficient as compared with attached wing but takes the advantage f ease in manufacturing. This study can be extended considering the thickness of the delta wing. Other geometries of the wing, i.e. rectangular wing can also be considered. In addition, taking the conjugate heat transfer ill make it closer to the real problem [64].

A disadvantage of PFHEs is that they are prone to fouling due to their small flow channels. They cannot be mechanically cleaned and require proper filtration for operation with potentially-fouling streams. The manufacturing cost of PFHEs is often higher than conventional heat exchangers due to a higher level of detail required. However, the total costs can be reduced by the cost saving due to the heat transfer enhancement.

Most PFHEs still use brazing to assemble the core. Recently, Rolls Laval Heat Exchangers Ltd. applied a technique developed for the cost-effective manufacture of aero-engine components to the construction of PFHEs. This heat exchanger is a PFHE employing a different manufacturing procedure–diffusion-bonding followed by super-plastically forming (SPF/DB), which allows a wide range of internal geometries to be produced, except for the conventional fin arrangements and perforated variants [65]. It has an area density of 700–800 m^2/m^3. The bond strength of the SPF/DB core is that of the parent metal, and very high containment pressures can be sustained. However, the porosity is similar to the brazed PFHE, typically about 0.6–0.75 [40]. Typical channel heights are about 2–5 mm.

The brazed PFHE has high area density of 1000–1500 m^2/m^3 (hydraulic diameter of the order of 1–2 mm) [66] and the ability to handle several streams. Typically, the effective heat transfer surface area is over 5 times greater than that of a conventional shell-and-tube heat exchanger. Although typical fin densities are 120–800 fins/m, applications exist for as many as 2100 fins/m. Common fin thickness ranges 0.15–0.61 mm, fin heights 3.8–12 mm. and fin pitch 1.15–4.5 mm [55]. A PFHE with 600 fins/m provides an area density of approximately 1300 m^2/m^3. PFHEs have been built with a surface area density of up to 5900 m^2/m^3.

The PFHE would be approximately 10% of the volume of an equivalent shell-and-tube heat exchanger with 19 mm tubes [67], and 5 times lighter in weight.

Very close temperature approaches between streams (typically 1–2 °C) can be accommodated leading to operational cost savings [51]. Heat transfer for the corrugated channel is enhanced by a factor of 2.5 compared to a conventional straight channel. Flow interruptions (as in offset strip fins, louvered fins, etc.) may increase the heat transfer coefficient 2–4 times that for the corresponding plain fin surface. For equal strip width, the louvered fin geometry provides enhancement comparable to that of offset strip fins.

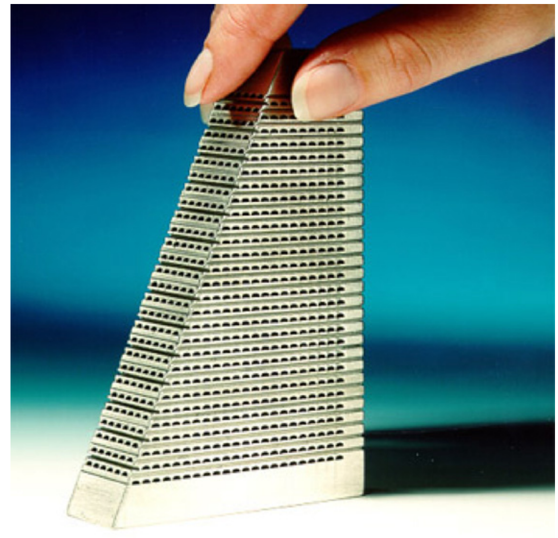


Fig. 4. Printed Circuit Heat Exchanger (courtesy of Heatric).

A variety of materials can be used in these heat exchangers such as aluminium, stainless steels, nickel, copper, ceramics, etc. depending upon the operating temperatures and pressures. PFHEs with aluminium or aluminium alloys as the principal core material are able to provide higher heat transfer efficiency and reduce the weight of the equipment when operating at a lower temperature. The diffusion-bonded PFHEs currently available are constructed using titanium. Several other commercially significant alloys exhibit super-plasticity, and the technique can be developed for use with both stainless steel and nickel alloys.

Operating limits of PFHEs depend upon the materials of construction. The upper temperature limits on aluminium brazed PFHEs are about 200 °C, stainless steel variants 800 °C, titanium superplastic-formed types 550 °C. For very high temperature (gas turbine heat recovery) a ceramic PFHE has also been developed for temperatures up to about 1150 °C with a peak temperature of 1370 °C [68].

With regard to pressures, aluminium brazed units can tolerate up to 120 bar, stainless steel units 80 bar. The braze material is nickel, cupronickel, silver or copper according to process stream compatibility (largely temperature) and other considerations. Higher pressures can be tolerated by using a diffusion-bonded structure, which in comparison has far greater integrity than a brazed construction. Use of stainless steel allows design pressures up to 620 bar are achievable and up to 400 bar with titanium [40,67].

2.3. Printed circuit heat exchanger (PCHE)

A PCHE (Fig. 4) is a relatively new concept originally invented as a result of research performed at the University of Sydney in the early 1980s. It has only been commercially manufactured by Heatric Ltd. (UK) since 1985. Interestingly, the PCHE was virtually unmentioned in the heat exchanger literature until the late 1990s [69].

As the name PCHE implies, the same technique is applied as the one used for manufacturing printed circuit boards in the electronics industry. In the first step of the manufacturing process, fine grooves are photo-chemically etched into one side of a flat



Fig. 5. Different types of PCHE.

metal plate forming the fluid passages. The etched-out plates are thereafter alternately joined by diffusion bonding, which is the second step and results in compact, extremely strong, all-metal heat exchanger cores. The diffusion bonding process includes a thermal soaking period to allow grain growth, thereby essentially eliminating the interface at the joints, which in turn gives base-material strength and very high pressure containment capability throughout the entire exchanger, in addition to the avoidance of corrosion cells. Because of diffusion bonding, its expected lifetime exceeds that of any other heat exchanger, based on a brazed structure [70]. The complete heat exchanger core is composed by welding together as many of these blocks as the thermal duty (flow capacity) of the heat exchanger requires.

The most commonly employed flow configurations include counter-flow, cross-flow, co-flow, or any combination of these. Several unique characteristics contribute to the superior performance of the PCHEs.

The conventional continuous zigzag PCHE flow paths do not allow the boundary layer growth and encourage turbulent flow. By enhancing heat transfer area and increasing local flow velocity at channel bending points, this zigzag channel shape enhances the heat transfer performance compared with the heat exchangers that have straight channels [71]. Compared to straight ducts, wavy geometries provide little advantage at low Reynolds numbers, and maximum advantage at transitional Reynolds numbers. Pra [72] and Gschwind [73] described the important flow mechanisms associated with wavy channels: At low Re < 200, steady recirculation zones form in the troughs of the wavy passages and heat transfer is not enhanced; for higher Reynolds numbers, the free shear layer becomes unstable; vortices roll up and are advected downstream, thus enhancing the heat transfer. However, at higher Reynolds numbers, periodic shedding of transverse vortices increases the Nusselt number with a considerable increase in the friction factor.

Flexibility is another distinguishing feature of PCHE. The versatility is particularly shown in the area of allowed fluid types and flow configurations. The variety of fluids for which PCHEs includes single-phase liquids, gases, and boiling and condensing two-phase flow. The design also allows multi-fluid integration (multi-stream capacity).

In addition to the wide operating range, the great potential of the PCHE is also illustrated by its enhancing safety features. As a result of its construction, it does not use or contain any gaskets or braze material. Consequently, the risk of leaks or fluid incompatibility is substantially reduced. In particular, the risk of leaks in a PCHE is approximately two orders of magnitude lower than for any other heat exchanger thanks to its continuous passage [74]. For gas-gas applications, fouling does not constitute a significant problem in PCHEs. As a result of high operating temperature, the amount of moisture present to agglomerate particles is negligible or even nonexistent, leaving the micro-channels free from discontinuities [70]. Consequently, there are no dead spots in the straight channels where particles would be prone to adhere to the passage wall and cause serious fouling problems.

The main limitation of PCHE is the pressure drop, which is roughly inversely proportional to the channel diameter. For high pressure applications, the pressure drop is not a constraint, but for low or moderate pressure applications, it will be the main barrier to the use of such heat exchangers. Each flow channel is regarded as a small pipe with many bends. In a bent pipe, swirl flows, reversed flows, and eddies occur around a bend corner, thereby the pressure drop in the channels is too larger due to reduction of hydraulic diameter, longer flow path length of zigzag channels and existence of separated flow at channel bending points [75]. In Brayton cycle, the pressure drop in channels of heat exchanger is closely connected with cycle efficiency. Hence, at the view of cycle efficiency, a heat exchanger design which can reduce pressure drop in channels is necessary [71].

PCHE falls within the category of CHEs because of its high surface density area (>2500 m^2/m^3) [36]. The plate size can be up to 1.2 m × 0.6 m [51]. The fluid passages are approximately semicircular in cross-section, being typically 1.0–2.0 mm wide and 0.5–1.0 mm depth [76,77] and giving 0.5–2.0 mm hydraulic diameters. For PCHE, the reduction of hydraulic diameter is not limited by the manufacturing cost increment rather than the factors such as the fluid used and the relationship between heat loads and pressure drop. The 'land' between passages is about 0.5 mm, the actual value being dependent on the pressure containment requirements.

PCHE is sometimes categorized as a PFHE with the fin of decreasing thickness towards the tip (at the plate join). Strictly-speaking, PCHE has only primary heat transfer surface, as do PHEs. That gives PCHE to a higher thermal performance than PFHE. Reduction of the hydraulic diameter results in decreased active flow length or heat exchanger size at the same Colburn j factor, Prandtl number and number of thermal units [40]. Such reductions are not achieved easily in usual PFHE because plate fin manufacturing and brazing bonding costs increase with increase of fin density or reduced hydraulic diameter. PCHE can achieve high thermal effectiveness of over 98% in a single unit.

Southall et al. [78] compared the heat transfer coefficient and friction factor of various fins and some compact heat transfer surfaces in PCHE. The high zigzag PCHE has the highest Colburn j factor, followed by the Serrated PFHE. The performance of PCHEs is generally better than the fin types.

A new PCHE with S-shaped fins (Fig. 5b) are proposed and compared with several fins in PFHEs and zigzag fin in PCHEs [75,79,80]. The Nusselt number of the PCHE with zigzag fins is 24–34% higher than that of S-shaped fins, but the pressure-drop is 4–5 times larger, depending on Reynolds number. The S-shaped model decreases the

pressure drop to 1/5 of the conventional zigzag model while giving identical heat transfer performance.

Kim et al. [81] investigated on thermal–hydraulic performance of a new PCHE model which has several airfoil shape fins (Fig. 5c). Because of the increased heat transfer area and the streamlined shape of the airfoil fins, this new PCHE model obtained the same heat transfer performance and a pressure drop only 1/20 as great as in the conventional zigzag channel PCHE.

The porosity of PCHE is low-of the order of 0.4–0.55, compared with 0.6–0.75 as a typical range for a PFHE of similar material. Because of the compactness provided by its design, the volume of PCHEs are typically 4–6 times smaller and lighter than conventional shell-and-tube heat exchangers designed for the same thermal duty and pressure drop.

With respect to mass, PCHE has an average mass-to-duty ratio in tones/MW of 0.2, as compared to 13.5 for a shell-and-tube heat exchanger [70]. Obviously, this reduction in size will cut the material and handling cost noticeably.

To allow operation under such extreme conditions, the materials commonly employed in PCHE include stainless steel 316L, Duplex and higher stainless steel alloys, titanium, copper and nickel (pure/alloys), all of which are corrosion resistant. Carbon steel is typically not used for two reasons [40]. First, because of the small channel diameter, the heat exchangers are designed for essentially zero corrosion allowance in order to avoid channel blockage. Second, carbon steel is unsuitable for diffusion bonding.

The PCHE concept allows simultaneous high temperature and high pressure operation with relatively thin wall thicknesses between the primary and secondary coolants. They are able to operate at pressures up to 500–1000 bar, generally 600 bar and can cope with extreme temperatures, ranging from cryogenic to 900 °C.

2.4. The Marbond heat exchanger

The flexibility of design and the high strength offered by the techniques used in construction gave PCHE a unique place in industry. Now, however, Chart Marston's Marbond heat exchanger, which is the latest truly innovative design to enter the CHE marketplace, challenges the PCHEs.

The manufacturing procedures of Marbond heat exchanger are similar to those of the PCHE. It is formed of slotted flat plates which have been chemically etched through. The plate pack is then diffusion-bonded together.

In contrast with the PCHE, several, thinner, slotted plates are typically stacked to form a single sub-stream, thus giving the potential for very low hydraulic diameters, depending on the width of the slots and the plate thickness [40], which significantly increases the porosity of the heat exchanger core.

It has inherent flexibility in terms of flow-path geometry, number of streams and the nature of the streams as other chemically etched and diffusion-bonded heat exchangers. It is clear that the form of surface is very versatile, giving precise passage shapes from a form very similar to that of a PFHE, to one similar to a PCHE surface [40]. And the type can be used for a wide variety of duties involving single phase or two phase streams, as well as for reactions.

In Marbond micro-channel reactors for catalytic hydrogenation, savings in energy are projected to be reflected in a 70% of original steam demand, 90% of electricity demand and 10% less feedstock. Some of the energy benefits arise due to a reduction in waste of 70% [82].

Produced by Chart Marston at their UK factory, the unit is about the size of a lap-top computer with channels about 1 mm hydraulic diameter (variants with hydraulic diameters down to 0.33 mm have been tested) [83]. The porosity is typically 0.6–0.7 [40]. In appropriate applications, it has a substantially higher area density than the PCHE. For example, a doubling of porosity, other factors being equal, results in a halving of the volume for a given surface area [67].

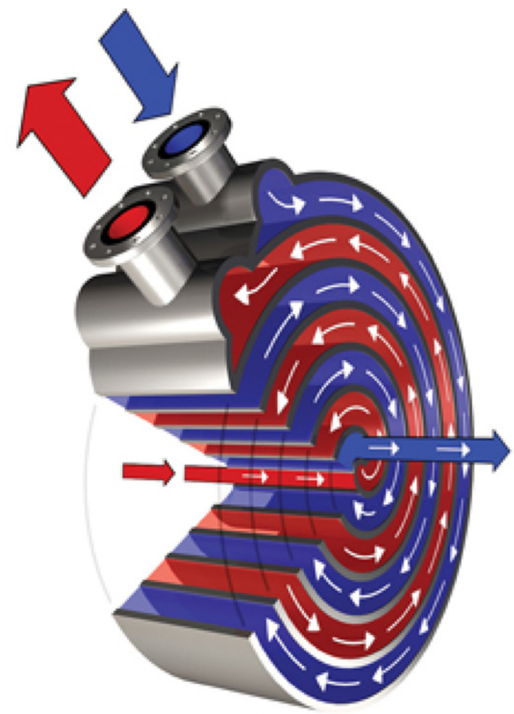


Fig. 6. Spiral heat exchanger (courtesy of Alfa Laval).

As with the PCHE, the range of constructional materials is only limited by their ability to be diffusion-bonded. The MarBond heat exchanger can be fabricated in stainless steel, titanium, higher alloy steels and Nickel [40]. The wide choice of materials allows for operation in potentially corrosive environments.

The MarBond heat exchangers are considered as high-integrity, high compact units able to operate over a range of pressures and temperatures not met in more conventional gasketed or welded CHEs. The Marbond unit is capable of being used at temperatures within the range −200 °C to 900 °C. Pressure differentials in excess of 400 bar can be accommodated [67].

2.5. Spiral heat exchanger

The spiral heat exchanger (SHE) has a long history as a heat exchanger type used for extensive applications from dirty fluids to high vacuum condensation.

A SHE refers to a helical tube configuration; more generally, the term refers to a circular heat exchanger with two long metal strips of plate rolled together to form a pair of concentric spiral channels of rectangular cross-section, one for each fluid (Fig. 6). The passages can be either smooth or corrugated, in some cases studs are welded onto one side of each strip to fix the spacing between the plates, provide mechanical strength and induce turbulence that increases heat transfer.

Alternate passage edges are sealed either by welding at each side of the channel [40] or by providing a gasket at each end cover to obtain the following arrangements of the two fluids: (1) both in spiral counter-flow; (2) one in spiral flow, the other in cross-flow across the spiral; or (3) one in spiral flow, the other in a combination of cross-flow and spiral flow. SHEs, being countercurrent, can have an LMTD correction factor of 1.0 and thus, do not have an LMTD penalty [84].

Table 3
Operating conditions of compact heat exchangers.

Technology	Maximum pressure, bar	Maximum temperature, °C
Gasketed PHE	35	200–250
Brazed PHE	45	225
AlfaRex PHE	40	350
Compabloc PHE	45	350
Shell & Plate	200	950
Hybrid PHE	80	900
PFHE	120	800
Ceramic HE	10	1300
Diffusion bonded PFHE	620	800
PCHE	500–1000	900
Marbond	400	900
SHE	25	540

The heat transfer coefficients in a SHE, if its plates are not corrugated, are not as high as in a PHE. However, it is higher than that in a shell-and-tube heat exchanger. The fluid in a SHE is fully turbulent at a much lower velocity than in straight tube heat exchangers because of the studs and the concentric shape of the flow passages. Due to the curvature of the passages, a centrifugal force is generated as the fluid flows. Secondary flow effects (eddy currents and vortices) induced by the centrifugal force significantly enhances the heat transfer rate [85].

Heat transfer characteristics of a SHE can be improved through adjusting channel dimensions, such as by changing the diameter and surface modification by adding roughness to the channel walls.

A SHE has a relatively large diameter. Channel spacing range between 5 mm and 25 mm (representing hydraulic diameters of 10–50 mm) is available, so that the designers can tradeoff between high heat transfer surface area density and a low propensity for blockage by fouling. Picon-Nunez et al. [86] present a shortcut method for the sizing of spiral plate heat exchangers with single-phase processes.

Strictly speaking, most of SHEs are not compact, but some recent developments are compact. The internal void volume is lower (less than 60%) than in a shell-and-tube heat exchanger [6], and this yields a compact and space-saving construction that can be readily integrated in any plant and reduces installation costs. The heat transfer surface ranges from 0.05 m^2 for refrigeration applications up to about 500 m^2 with a maximum shell diameter of 1.8 m and the sheet metal thickness range is 1.8–4 mm for industrial processes [51]. The surface area requirement is about 20% lower than that for a shell-and-tube unit for the same heat duty [6].

Recently the newly designed Swiss-roll recuperator based on a spiral concept is proposed as a heat exchanger to recover the exhaust heat for future higher efficiency microturbines. The strategies to have a Swiss-roll recuperator of higher efficiency, low pressure loss and compact size were discussed and the feasibility studies were performed by Shih et al. [87,88]. The proposed unit potentially has a compact size and a thermal efficiency higher than 20% for the power output less than 10 kW, and it has granted the U.S. patents [89]. In another design of spiral type of recuperator, the gas side is finned with plain fins, and the other side has many various ribs or protrusions on the sheet [90,91]. Swiss-roll combustors were also numerically studied by Kuo et al. [92]. They developed a CFD model and compare its predictions to experiments over wide Re ranges.

SHEs are often used in the heating of high viscosity and dirty fluids. It exhibits lower tendency to fouling. This is due to the particular geometry that creates a constant change in direction thus increasing local turbulence that removes any likelihood of dead spots and stagnation [86]. The fouling causes a localized increase in fluid velocity, increasing the drag on the fouled surface, thus helping to scrap off and dislodge the blockage and keep the SHE clean. The mechanical design of the SHE also enables easy maintenance and simplified inspection. When a SHE requires cleaning, all heat transfer surfaces are readily accessible by simply removing the heads.

No insulation is used outside this heat exchanger because of the cold fluid flowing in the outermost passage, resulting in negligible heat loss, if any, due to its inlet temperature closer to the ambient temperature [6].

Exceptional compactness, self-cleaning design, no insulation and minimum maintenance costs make SHEs frequently the most cost-effective solution.

The materials of construction are generally carbon steel, stainless steel, titanium, or any other metal that can be cold formed, rolled, and welded. Hastelloy and Incoloy and high-nickel alloys units are also available [67].

SHEs have been designed for operation at temperatures up to 540 °C, but conventionally most are designed to operate up to 200 °C. As with gasketed PHEs, the temperature limit is a strong function of the gasket material used to seal the gaps between the open channel ends and the end covers. Some manufacturers quote design pressures of less than 6 bar. Other units are designed to operate up to 25 bar [67].

2.6. Ceramic heat exchanger

Commercial CHEs are mostly fin-and-tube or plate-type designs using copper or aluminium. However, the advances in ceramics materials, especially in recent 20 years, help the development of novel ceramic CHE designs in high temperature applications. Ceramic material is defined as something having a glazed or unglazed body of crystalline or partly crystalline structure, or of glass, which body is produced from essentially inorganic, non-metallic substances and either is formed from a molten mass which solidifies on cooling, or is formed and simultaneously or subsequently matured by the action of the heat [93].

Currently ceramic CHEs are primarily constructed by replacing the materials for parts of existing CHEs with ceramic. The main parts considered for replacement are tubes and fins. The manufacturing procedures include forming primary components from raw materials, subsequent machining, joining, bonding, and assembling, which can be further classified as monolithic and non-monolithic assembly. Because the individual components are bonded together permanently without internal joint, there is no sealing problem in monolithic assembly, but stress concentrations can arise under extreme operating conditions. In non-monolithic assembly, individual components can be disassembled and repaired. However, sealing problem must be considered because of the brittleness of ceramics and the difficulties of forming a resilient metal–ceramic or ceramic–ceramic joint due to the differences in the coefficient of thermal expansion of the two materials [94]. Therefore some advanced fabrication techniques like laser supported brazing [95,96] are often used and further studied to maximize the benefit and broaden the application of ceramic materials in heat exchangers.

The main advantages for ceramic materials over traditional metallic materials in CHE construction are their extremely high temperature stability, low material cost and excellent corrosion resistance. The ceramic-based CHEs can withstand operating temperatures that far exceed those of conventional metallic alloys, Silicon carbide (SiC) 1400 °C, Silicon nitride (Si_3N_4) 1900 °C, Alumina 1500–1700 °C, and Aluminium nitride (AlN) 1300 °C [94]. At elevated operating temperatures, ceramic CHEs possess high fouling resistance and resistance to corrosion and chemical erosion.

The major obstacles in the improvement of ceramic CHEs mainly embodies in their intrinsic brittleness in tension, difficulties in shaping and sealing and thus high manufacturing costs. They

cannot withstand large thermal gradients and are susceptible to thermal shock failure except silicon carbide and silicon nitride. Therefore, major of the researches focuses on less brittle ceramics forms such as composite ceramics. Ceramic matrix composites (CMCs) were developed by combining reinforcing ceramic phases within a ceramic matrix to meet the specific requirements including high thermal shock resistance, high hardness, non-magnetic and nonconductive properties. The most commonly used CMCs are nonoxide CMCs namely carbon/carbon (C/C), carbon/silicon carbide (C/SiC), and silicon carbide/silicon carbide (SiC/SiC) [94].

Compared to ceramics materials, metallic CHE has the advantages of easy to fabricate, high material strength and great compactness with extended surfaces. To overcoming the shortcomings of ceramic heat exchanger, a hybrid heat exchanger is in research by combining ceramic and metallic heat exchanger cores, which is expected to have the advantages: low cost, high effectiveness, modular manufacture, reduced temperature gradients on ceramic, thermal expansion unrestrained.

Among the ceramics materials, SiC ceramics that have been extensively investigated [97] are the major focus of R&D today. SiC has been treated as a promising material for high-temperature heat exchanger applications, primarily because of its excellent thermal stability and corrosion resistance in severe environments, and sufficient thermal conductivity at elevated temperature [98].

Steen [99] investigated the short and long term mechanical properties of a sintered silicon carbide intended as a heat exchanger material in advanced gas turbine containing coal-fired power plants.

Amirthan et al. [100] prepared four different types of Si/SiC ceramic composites by liquid silicon infiltration technique and measured their thermal conductivities at different temperatures by the laser flash thermal conductivity method. They found that the presence of free carbon and voids are notably affecting the thermal conductivity of these materials.

The investigation of ceramic CHEs involved liquid-to-liquid heat exchangers [101], liquid-to-gas heat exchangers, gas-to-gas heat exchangers [102–104], heat sinks and volumetric solar receivers.

Schulte-Fischedick et al. [102] proposed a sintered SiC ceramic PFHE coated with an environmental barrier coating based on the “Offset Strip Fin” design. They studied it as high temperature heat exchanger in the externally fired combined cycle (EFCC) or other applications that need extreme operation temperatures up to 1250 °C. The thermal design was conducted by using empirical correlations drawn from the literature via the LMTD-method, while the stress distribution of the selected design during operation was investigated by means of finite element method (FEM).

Islamoglu [103,104] analyzed the temperature distribution for steady-state heat transfer and the thermal stresses induced by temperature difference in a silicon carbide (SiC) ceramic tube of heat transfer equipment. The temperature and the stress fields were computed by Finite element method (FEM). The effects of annular fin with different profiles (rectangular and triangular) [103] and the axial non-uniform convective heat transfer coefficient [104] on the temperature and thermal stresses have been investigated.

Volumetric solar receivers consist of high-porosity materials and are used in the solar tower technology for the conversion of concentrated solar radiation into heat. Fend et al. [105] measured thermal conductivity, convective heat transfer coefficient and efficiency of selected materials made from various oxide and non-oxide ceramics, ceramic foams and metal structures, and they also experimentally investigated how the properties of the porous materials affect flow stability. It was concluded that a possible introduction of materials based on ceramic foams and ceramic fabrics in solar tower technology would offer the potential for a more effective and reliable operation compared to the current open volumetric receiver technology. They presented and tested two novel porous materials for an application as a volumetric receiver: a double-layer silicon carbide foam and a screen-printed porous silicon carbide material. Both ceramic technologies are future options with properties required for the use as a high-performance solar receiver [106].

A few heat transfer applications were suggested where ceramic materials in heat exchangers may hold substantial relevance and potential merit: evaporators in evaporative cooling systems for air-conditioning, recuperators and generators in $LiBr/H_2O$ absorption chillers for air-conditioning, primary heat exchangers in gas-fired furnaces for space heating, high temperature recuperators and chemical digesters, open-cell foams for reactive heat exchange processes and filtration. However, many of these proposed applications, only based on simulation results, have not been sufficiently studied. Thus, some related research programs are just launched aimed at comprehensive study of the use of these emerging materials [107].

3. Comparison of heat transfer enhancement technologies in compact heat exchangers

3.1. Comparison on the capabilities to cope with the operating conditions

When the use of a CHE is a possibility in a process or other applications, often, it is preferable that the principal features of CHEs largely confine the choice of type and its surface to a small selection. Plate-fin and tube-fin heat exchangers are the representatives of CHEs for gas flow on one or both fluid sides, and gasketed, brazed, welded PHEs and PCHEs are examples of CHEs for liquid flow. Table 3 summarizes the principal features of different types of CHEs. This indicates the operational temperature and pressure ranges available for each type.

3.2. Comparison on the thermo-hydraulic performance

Performance of a heat exchanger depends upon the heat transfer between the working fluids flowing through it. Heat transfer rate for turbulent flow is higher than that for laminar flow and different technologies are used to enhance heat transfer by introducing turbulence, better fluid mixing and so on. However, any technology that enhances heat transfer is most likely to increase pressure drop also, and it is a common knowledge that the ratio of pressure drop increase is often larger than the ratio of heat transfer enhancement.

3.2.1. The results of the comparison on the thermo-hydraulic performance

To account for the pressure drop in the performance of CHE, a performance evaluation plot has been recently proposed by Fan et al. [108]. In their plot, different enhanced techniques for the same reference system can easily and clearly be compared for their energy-saving performances. For some techniques which lead to the reduction of both heat transfer rate and friction factor, the proposed plot is still applicable. This plot will be useful in the study of heat transfer enhancement technique oriented for energy-saving purposes.

Based upon the available correlations of heat transfer and friction factor developed by various investigators quoted in the open literature, this plot is applied to compare the thermo-hydraulic performance of different heat transfer enhancement technologies in CHEs. These correlations along with the range of parameters investigated are given in Table 4 , and the plot is shown in Fig. 7.

In the plot (Fig. 7) the ratio of the friction factor of the enhanced design over that of the reference one (f_0) and the ratio of the related heat transfer enhancement at the same Reynolds number (Nu_0) are

Table 4
Correlations developed for heat transfer and friction factor for different heat transfer enhancement techniques used in CHEs.

Author	Types of roughness	Range of parameters	Correlations: Friction factor	Correlations: Heat transfer coefficient
Prasad and Saini [109]	Small diameter transverse wires on top plate	e/D: 0.020–0.033 p/e: 10–20 Re: 5000–50,000	$\bar{f} = \frac{(W+2B)f_s+Wf_r}{2(W+B)}$ $f_r = \frac{2}{\left[0.95\left(\frac{p}{e}\right)^{0.53}+2.5\ln\left(\frac{D}{2e}\right)-3.75\right]^2}$	$\overline{St} = \frac{\bar{f}/2}{1+\sqrt{\bar{f}/2}\left[4.5(e^+)^{0.28}Pr^{0.57}-0.95\left(\frac{p}{e}\right)^{0.53}\right]}$
Hwang and Liou [110]	Staggered parallel rectangular ribs on top and bottom plates	2A: 160 mm 2B: 40 mm Rib angle-of-attack: 90° PR: 5–20 H/De: 0.081, 0.162 H/2B: 0.13, 0.26 Open-area ratio of the perforated rib: 50% Re: 10,000–50,000	$R(H^+) = \left(\frac{f}{8}\right)^{-0.5} + 2.5\ln\left[\left(\frac{2H}{De}\right)\left(\frac{2A}{A+B}\right)\right] + 2.5$ $R = 3.31\left(\frac{PR}{10}\right)^{0.53}$ for the solid-type rib $R = 5.15\left(\frac{PR}{10}\right)^{0.53}$ for the perforated rib	$G(H^+, Pr) = \left(\frac{f}{8}\right)^{-0.5}/St + 2.5\ln\left[\left(\frac{2H}{De}\right)\left(\frac{2A}{A+B}\right)\right] + 2.5$ $G = 3.72(H^+)^{0.35}\left(\frac{PR}{10}\right)^{0.08}$ for the solid-type rib $G = 2.25(H^+)^{0.35}\left(\frac{PR}{10}\right)^{0.08}$ for the perforated rib $H^+ = \frac{H}{De}Re\left(\frac{f}{8}\right)^{0.5}$
Liou and Wang [111]	Detached square ribs near bottom plate	Duct width: 160 mm Duct height: 40 mm Aspect ratio: 4 Rib height: 5.2 mm Rib width: 5.2 mm Rib angle-of-attack: 90° The ratio of rib pitch to height: 10 The rib to duct height ratio: 0.13 The non-dimensional clearance Between rib and wall: 0.58 Re: 5000–50,000	$f = 5.979\mathrm{Re}^{-0.363}$	$\overline{Nu_P} = 0.364Re^{0.604}$
Gupta et al. [112]	Angled circular ribs on top plate	Test length: 1500 mm W: 200 mm H: 19 mm e/D: 0.023–0.05 p/e: 7.5&10 α: 30–90° Re: 4000–18,000	$f = 0.1911\left(\frac{e}{D}\right)^{0.196}\left(\frac{W}{H}\right)^{-0.093} \times Re^{-0.165}e^{-0.993(1-\alpha/70)^2}$	$h = 0.0024\left(\frac{e}{D}\right)^{0.001}\left(\frac{W}{H}\right)^{-0.06} \times Re^{1.084}e^{-0.04(1-\alpha/60)^2}\left(\frac{k}{D}\right)$ for $e^+ < 35$ $h = 0.0071\left(\frac{e}{D}\right)^{-0.24}\left(\frac{W}{H}\right)^{-0.028} \times Re^{0.88}e^{-0.475(1-\alpha/60)^2}\left(\frac{k}{D}\right)$ for $e^+ \geqq 35$
Leung et al. [113]	Rectangular ribs on bottom plate	Duct width: 202 mm Duct height: 120 mm Rib angle-of-attack: 90° Rib length: 200 mm B: 6.35 mm Spacing between ribs: 6.35 mm L/B: 3, 4 H/B: 6, 8, 10 Rec: 510–2050	$f_C = 0.79Re_C^{-0.77}\left(\frac{H}{B}\right)^{1.98}\left(\frac{L}{B}\right)^{-0.79}$	$Nu_C = 0.55Re_C^{0.23}\left(\frac{H}{B}\right)^{0.77}\left(\frac{L}{B}\right)^{0.24}$
Saini and Saini [114]	Expended wire mesh on top plate	Test length: 1000 mm W: 405 mm H: 35 mm e/D: 0.012–0.039 L/e: 25.00–71.87 S/e: 15.62–46.87 Re: 1900–13,000	$f = 0.815Re^{-0.361}\left(\frac{L}{e}\right)^{0.266}\left(\frac{S}{10e}\right)^{-0.190}\left(\frac{10e}{D}\right)^{0.591}$	$Nu = 4.0\times10^{-4}Re^{1.22}\left(\frac{e}{D}\right)^{0.625}\left(\frac{S}{10e}\right)^{2.22} \times e^{-1.25\left[\ln\left(\frac{S}{10e}\right)\right]^2}\left(\frac{L}{10e}\right)^{2.66}e^{-0.824\left[\ln\left(\frac{L}{10e}\right)\right]^2}$

Table 4 (*Continued*)

Author	Types of roughness	Range of parameters	Correlations	
			Friction factor	Heat transfer coefficient
Tsia and Hwang [115]	Alternate attached-detached ribs near bottom plate	2W: 160 mm 2B: 40 mm W/B: 4 h: 8 mm Rib width: 8 mm Rib angle-of-attack: 90° Detached rib clearance: 4 mm Pi/h: 10–30 h/2B: 0.2 The ratio of the rib clearance to h: 0.5 Re: 12,000–70,000	$R(h^+) = \left(\frac{f}{8}\right)^{-0.5} + 2.5\ln\left[\left(\frac{2h}{D_e}\right)\left(\frac{2W}{W+B}\right)\right] + 2.5$ $R = 2.9\left(\frac{P_i}{10h}\right)^{0.53}$	$G(h^+, Pr) = \left(\frac{f}{8}\right)^{-0.5}/St + 2.5\ln\left[\left(\frac{2h}{D_e}\right)\left(\frac{2W}{W+B}\right)\right] + 2.5$ $G = 2.9(h^+)^{0.28}\left(\frac{P_i}{10h}\right)^{0.07}$ $h^+ = \frac{h}{D_e} Re\left(\frac{f}{8}\right)^{0.5}$
Karwa et al. [116]	Rectangular and chamfered repeated ribs on bottom plate	W: 150 mm H: 12.5–30 mm W/H: 4.8–12 Test length to D_h ratio: 32, 66 e/D_h: 0.014–0.032 p/e: 4.5–8.5 Φ: −15° to 18° Re: 3000–20,000	$R = \sqrt{\frac{2}{f}} + 2.5\ln\left(\frac{2e}{D_h}\right) + 3.75$ $R = 1.66e^{-0.0078\phi}\left(\frac{W}{H}\right)^{-0.4}\left(\frac{p}{e}\right)^{2.695} e^{-0.762\ln\left(\frac{p}{e}\right)^2}(e^+)^{-0.075}$ for $5 \leqq e^+ < 20$ $R = 1.325e^{-0.0078\phi}\left(\frac{W}{H}\right)^{-0.4} \times \left(\frac{p}{e}\right)^{2.695} e^{-0.762\ln\left(\frac{p}{e}\right)^2}$ for $20 \leqq e^+ \leqq 60$ For W/H > 7.75 use W/H = 7.75 in equations $e^+ = \sqrt{\frac{f}{2}} Re \frac{e}{D_h}$	$g = \left(\frac{f}{2nd} - 1\right)\sqrt{\frac{2}{f}} + R$ $g = 103.77e^{-0.006\phi}\left(\frac{W}{H}\right)^{0.5}\left(\frac{p}{e}\right)^{-2.56} e^{0.7343\ln\left(\frac{p}{e}\right)^2}(e^+)^{-0.31}$ for $7 \leqq e^+ < 20$ $g = 32.26e^{-0.006\phi}\left(\frac{W}{H}\right)^{0.5}\left(\frac{p}{e}\right)^{-2.56} e^{0.7343\ln\left(\frac{p}{e}\right)^2}(e^+)^{0.08}$ for $20 \leqq e^+ \leqq 60$ when W/H > 10 use W/H = 10 in equations
Verma and Prasad [117]	Circular ribs on top plate	e/D: 0.01–0.03 p/e: 10–40 Re: 5000–20,000 e+: 8–42	$f_r = 0.245\left(\frac{p}{e}\right)^{-0.206}\left(\frac{e}{D}\right)^{0.243} Re^{-1.25}$	for $e^+ \leqq 24$ $Nu_r = 0.08596\left(\frac{p}{e}\right)^{-0.054}\left(\frac{e}{D}\right)^{0.072} Re^{0.723}$ for $e^+ > 24$ $Nu_r = 0.02954\left(\frac{p}{e}\right)^{-0.016}\left(\frac{e}{D}\right)^{0.021} Re^{0.802}$ $e^+ = \frac{e}{d}\sqrt{\frac{f_r}{2}} Re$
Momin et al. [118]	V-shaped wire ribs on top plate (downward)	Test length: 1.5 m Duct width: 0.2 m Aspect ratio: 10.15 e/D_h: 0.02–0.034 The ratio of rib pitch to height:10 α: 30–90° Re: 2500–18,000	$f_r = 6.266Re^{-0.425}\left(\frac{e}{D_h}\right)^{0.565}\left(\frac{\alpha}{60}\right)^{-0.093} \times e^{-0.719\ln\left(\frac{\alpha}{60}\right)^2}$	$Nu_r = 0.067Re^{0.888}\left(\frac{e}{D_h}\right)^{0.424} \times \left(\frac{\alpha}{60}\right)^{-0.077} e^{-0.782\ln\left(\frac{\alpha}{60}\right)^2}$

Table 4 (*Continued*)

Author	Types of roughness	Range of parameters	Correlations	
			Friction factor	Heat transfer coefficient
Bhagoria et al. [119]	Transverse wedge-shaped ribs on top plate	test length: 1600 mm W: 150 mm H: 30 mm W/H: 5 e/D_h: 0.015–0.033 $60.17\Phi - 1.0264 < p/e < 12.12$ Φ: 8–15° Angle of attack: 90° Re: 3000–18,000	$f_r = 12.44Re^{-0.18}\left(\frac{e}{D_h}\right)^{0.99}\left(\frac{p}{e}\right)^{-0.52}\left(\frac{\phi}{10}\right)^{0.49}$	$Nu = 1.89\times10^{-4}Re^{1.21}\left(\frac{e}{D_h}\right)^{0.426}\left(\frac{p}{e}\right)^{2.94} \times e^{-0.71\ln\left(\frac{p}{e}\right)^2}\left(\frac{\phi}{10}\right)^{-0.018}e^{-1.50\ln\left(\frac{\phi}{10}\right)^2}$
Chandra et al. [120]	varying number of transverse ribbed wall in square duct	W: 3.81 cm H: 3.81 cm L/D_h: 20 e/D_h: 0.0625 P/e: 8 Re: 10,000–80,000	$f_{rr} = f_r + \frac{C_s}{C_r}(f_r - f_{ss})$ $f_{ss} = 0.046Re^{-0.2}$ $R(e^+) = \left(\frac{f_{rr}}{2}\right)^{-0.5} + 2.5\ln\left(\frac{2e}{D_h}Z\right) + 2.5$ $R(e^+) = 3.44$ for $e^+ \geqq 120$ $e^+ = \frac{e}{D_h}Re\left(\frac{f_{rr}}{2}\right)^{0.5}$ $Z = \frac{2AR}{1+AR}$ $AR = \frac{W}{H}$	$St_{rr} = \left(\frac{C_r}{C}\right)^{-0.15}St_r$ $G(e^+) = \left(\frac{f_{rr}}{2}\right)^{0.5}/St_{rr} + 2.5\ln\left[\left(\frac{2e}{D_h}\right)Z\right] + 2.5$ $G(e^+) = (e^+)^{0.47}$ for $e^+ \geqq 120$
Chang et al. [121]	scale-roughened (top and bottom plates: in-line; in each plate: staggered)	Test length: 155 mm W: 80 mm H: 10 mm e: 1 mm Scale pitch: 10 mm Scale diameter: 10 mm Scale angle of attack: 11° Re: 1500–15,000	For forward flow $f = 2.679Re^{-0.318}$ For downward flow $f = 8.836Re^{-0.39}$	For forward flow $Nu = \left(0.0896 + 0.0596e^{-0.92\frac{x}{d}}\right)Re^{0.815}$ For downward flow $Nu = \left(0.169 + 0.638e^{-0.81\frac{x}{d}}\right)Re^{0.7}$
Jaurker et al. [122]	Rectangular rib-V grooved top plate	Test length: 1200 mm W: 156 mm H: 22 mm e/D: 0.0181–0.0363 p/e: 4.5–10 g/p: 0.3–0.7 Re: 3000–21,000	$f = 0.001227Re^{-0.199}\left(\frac{e}{D}\right)^{0.585}\left(\frac{P}{e}\right)^{7.19} \times \left(\frac{g}{P}\right)^{0.645}e^{-1.854\left[\ln\left(\frac{p}{e}\right)\right]^2} \times e^{1.513\left[\ln\left(\frac{g}{P}\right)\right]^2 + 0.8662\left[\ln\left(\frac{g}{P}\right)\right]^3}$	$Nu = 0.002062Re^{0.936}\left(\frac{e}{D}\right)^{0.349}\left(\frac{P}{e}\right)^{3.318} \times \left(\frac{g}{P}\right)^{1.108}e^{-0.868\left[\ln\left(\frac{p}{e}\right)\right]^2} \times e^{2.486\left[\ln\left(\frac{g}{P}\right)\right]^2 + 1.406\left[\ln\left(\frac{g}{P}\right)\right]^3}$

Table 4 (*Continued*)

Author	Types of roughness	Range of parameters	Correlations: Friction factor	Correlations: Heat transfer coefficient
Layek et al. [123,124]	Chamfered rib-V grooved Top plate	Test length: 1200 mm W: 150 mm H: 30 mm e/D_h: 0.022–0.04 P/e: 4.5–10 g/P: 0.3–0.6 Φ: 5–30° Re: 3000–21,000	$f = 0.00245Re^{-0.124}\left(\frac{e}{D_h}\right)^{0.365}\left(\frac{P}{e}\right)^{4.32}\left(\frac{g}{P}\right)^{-1.124} \times e^{0.005\phi}e^{-1.09\left[\ln\left(\frac{p}{e}\right)\right]^2}e^{-0.68\left[\ln\left(\frac{g}{P}\right)\right]^2}$ $f = 0.00276Re^{-0.1279}\left(\frac{e}{D_h}\right)^{0.3632}\left(\frac{P}{e}\right)^{4.255}\left(\frac{g}{P}\right)^{-0.976} \times e^{0.00575\phi}e^{-1.066\left[\ln\left(\frac{p}{e}\right)\right]^2}e^{-0.583\left[\ln\left(\frac{g}{P}\right)\right]^2}$	$Nu = 0.00225Re^{0.92}\left(\frac{e}{D_h}\right)^{0.52}\left(\frac{P}{e}\right)^{1.27} \times \left(\frac{g}{P}\right)^{-1.21}\phi^{0.24}e^{-0.22(\ln\phi)^2} \times e^{-0.46\left[\ln\left(\frac{p}{e}\right)\right]^2}e^{-0.74\left[\ln\left(\frac{g}{P}\right)\right]^2}$ $Nu = 0.0028Re^{0.93}\left(\frac{e}{D_h}\right)^{0.528}\left(\frac{P}{e}\right)^{2.17} \times \left(\frac{g}{P}\right)^{-1.054}\phi^{0.77}e^{-0.138(\ln\phi)^2} \times e^{-0.57\left[\ln\left(\frac{p}{e}\right)\right]^2}e^{-0.649\left[\ln\left(\frac{g}{P}\right)\right]^2}$
Karmare and Tikekar [125]	Staggered circular grit ribs on top plate	Test length: 1500 mm W: 250 mm H: 25 mm e/D_h: 0.035–0.044 p/e: 12.5–36 l/s: 1.72–1 Rib angle of attack: 45–60° Re: 3600–17,000	$f = 15.55Re^{-0.26}\left(\frac{e}{D_h}\right)^{0.91}\left(\frac{l}{s}\right)^{-0.27}\left(\frac{p}{e}\right)^{-0.51}$	$Nu = 2.4 \times 10^{-3}Re^{1.3}\left(\frac{e}{D_h}\right)^{0.42} \times \left(\frac{l}{s}\right)^{-0.146}\left(\frac{p}{e}\right)^{-0.27}$
Aharwal et al. [126]	Inclined rib with gap on top plate	Test length: 1200 mm W/H: 5.87 e: 2 mm e/D_h: 0.0377 Rib width: 2 mm p/e: 10 d/W: 0.167–0.5 g/e: 0.5–2 α: 45–60° Re: 3000–18,000	$f = 0.071Re^{-0.133}\left(\frac{p}{e}\right)^{1.83}e^{-0.44\left[\ln\left(\frac{p}{e}\right)\right]^2} \times \left(\frac{d}{W}\right)^{-0.43}e^{-0.14\left[\ln\left(\frac{d}{W}\right)\right]^2} \times \left(\frac{g}{e}\right)^{-0.052}\left(\frac{\alpha}{60}\right)^{0.67}e^{0.12\left[\ln\left(\frac{g}{e}\right)\right]^2}\left(\frac{e}{d}\right)^{0.69}$	$Nu = 0.0028Re^{1.08}\left(\frac{p}{e}\right)^{1.87}e^{-0.45\left[\ln\left(\frac{p}{e}\right)\right]^2}\left(\frac{\alpha}{60}\right)^{0.006} \times e^{-0.65\left[\ln\left(\frac{\alpha}{60}\right)\right]^2}\left(\frac{d}{W}\right)^{-0.32}e^{-0.12\left[\ln\left(\frac{d}{W}\right)\right]^2} \times \left(\frac{g}{e}\right)^{-0.03}e^{-0.18\left[\ln\left(\frac{g}{e}\right)\right]^2}\left(\frac{e}{d}\right)^{0.5}$
Varun et al. [127]	Inclined and transverse wire ribs on top plate	Test length: 1000 mm W: 290 mm H: 29 mm e/D_h: 0.03 p/e: 3–8 Inclined rib angle of attack: 60° Re: 2000–14,000	$f = 1.0858Re^{-0.3685}\left(\frac{p}{e}\right)^{0.0114}$	$Nu = 0.0006Re^{1.213}\left(\frac{p}{e}\right)^{0.0104}$

Table 4 (*Continued*)

Author	Types of roughness	Range of parameters	Correlations	
			Friction factor	Heat transfer coefficient
Chang et al. [128]	Staggered Parallel V-shaped ribs and deepened scales	Test length: 222 mm W: 80 mm H: 40 mm H/W: 1/2 d: 53 mm Rib angle of attack: 45° Rib height: 1.77 mm Rib pitch: 17.7 mm Rib land: 1.77 mm Scale angle of penetration: 11° Scale height: 1 mm Scale pitch: 10 mm Scale diameter: 10 mm Re: 1000–30,000	$C_f = 17.098\mathrm{Re}^{-0.449}$ (forward flow) $C_f = 17.17\mathrm{Re}^{-0.5}$ (backward flow)	$\overline{Nu} = 0.157Re^{0.787}$ (forward flow) $\overline{Nu} = 0.49Re^{0.649}$ (backward flow)
Saini and Verma [129]	Dimpled top plate	Test length: 1000 mm W: 300 mm H: 25 mm e: 0.8–1.7 mm e/D_h: 0.0189–0.038 p: 12–18 mm p/e: 8–12 d: 0.8–1.7 mm Re: 2000–12,000	$f_r = 0.642Re^{-0.423}\left(\frac{p}{e}\right)^{-0.465} e^{0.054\left[lg\left(\frac{p}{e}\right)\right]^2} \times \left(\frac{e}{D}\right)^{-0.0214} e^{0.840\left[lg\left(\frac{e}{D}\right)\right]^2}$	$Nu = 5.2\times10^{-4}Re^{1.27}\left(\frac{p}{e}\right)^{3.15} e^{-2.12\left[lg\left(\frac{p}{e}\right)\right]^2} \times \left(\frac{e}{D}\right)^{0.033} e^{-1.30\left[lg\left(\frac{e}{D}\right)\right]^2}$
Saini and Saini [130]	Arc shaped G. I. wires on top plate	Test length: 1000 mm W: 300 mm H: 25 mm e/d: 0.0213–0.0422 Roughness pitch/e: 10 Wire diameter: 1.4 mm $\alpha/90$: 0.3333–0.6666 Re: 2000–17,000	$f = 0.14408Re^{-0.17103}\left(\frac{e}{d}\right)^{0.1765}\left(\frac{\alpha}{90}\right)^{0.1185}$	$Nu = 0.001047Re^{1.3186}\left(\frac{e}{d}\right)^{0.3772}\left(\frac{\alpha}{90}\right)^{-0.1198}$
Bopche and Tandale [131]	Inverted U-shaped turbulators on top plate	Test length: 1000 mm W: 130 mm H: 22 mm e/D_h: 0.0186–0.03986 p/e: 6.667–57.14 Angle of attack of flow: 90° Re: 3800–18,000	$f_r = 1.2134Re^{-0.2076}\left(\frac{p}{e}\right)^{-0.4259}\left(\frac{e}{D_h}\right)^{0.3285}$	$Nu_r = 0.5429Re^{0.7054}\left(\frac{p}{e}\right)^{-0.1592}\left(\frac{e}{D_h}\right)^{0.3619}$

Table 4 (*Continued*)

Author	Types of roughness	Range of parameters	Correlations: Friction factor	Correlations: Heat transfer coefficient
Karwa and Maheshwari [132]	Half perforated baffles on top plate	Test length: 1.652 m W: 298.55 mm H: 38.4 mm W/H: 7.77 Thickness of baffle: 0.9 mm e: 19 mm p/e: 7.21 Open area ratio: 26% Angle of attack of flow: 90° Re: 2700–11,150	$f = 0.1673\mathrm{Re}^{-0.0213}$	$Nu = 0.0893\mathrm{Re}^{0.7608}$
Prasad et al. [133]	Packed with wire mesh	Test length: 2.4 m W: 400 mm H: 25 mm d_w: 1.06–1.48 mm p_t: 2.16–4.23 mm n: 5–11 P: 0.599–0.816 p_t/d_w: 2.04–3.47 $1/nP$: 0.152–0.263 r_h: 0.396–1.351 mm	$f_p = 3.5722\left(\frac{1}{nP}\right)^{1.0431}\left(\frac{p_t}{d_w}\right)^{1.1507}Re_P^{-0.43}$	$J_h = 0.2563\left(\frac{1}{nP}\right)^{0.609}\left(\frac{p_t}{d_w}\right)^{0.7954}Re_P^{-0.63}$
Varshney and Saini [134]	Packed with wire mesh screen matrix	Test length: 2.39 m W: 405 mm H: 25 mm d_w: 0.36–0.795 mm p_t: 2.08–3.19 mm p_t/d_w: 3.77–7.55 n: 5–14 P: 0.887–0.958 r_h: 1.403–2.994 mm $\mathrm{Re_p}$: 300–1500	$f_p = 2.484\left[\frac{1}{nP}\left(\frac{p_t}{d_w}\right)\right]^{0.699}Re_P^{-0.44}$	$j_h = 0.647\left[\frac{1}{nP}\left(\frac{p_t}{d_w}\right)\right]^{2.104}Re_P^{-0.55}$
Thakur et al. [135]	Packed with wire screen matrix	Test length: 2.4 m W: 400 mm H: 25 mm d_w: 0.79–1.4 mm p_t: 2.5–3.19 mm p_t/d_w: 2.14–4.01 n: 5–12 P: 0.667–0.880 r_h: 0.525–1.59 mm $\mathrm{Re_p}$: 182–1168	$f_p = 3.0\left[\left(\frac{1}{nP}\right)^{0.50}\left(\frac{p_t}{d_w}\right)^{0.25}\right]^{0.90}Re_P^{-0.41}$	$j_h = 0.4\left[\left(\frac{1}{nP}\right)^{0.50}\left(\frac{p_t}{d_w}\right)^{0.25}\right]^{1.4}Re_P^{-0.61}$
Kurtbas and Durmus [136]	Flat channel	Test length: 0.9 m W: 400 mm H: 25 mm	$11.353\mathrm{Re}^{-0.168}$	$0.122\mathrm{Re}^{0.612}$
	Onduline channel		$28.889\mathrm{Re}^{-0.199}$	$0.154\mathrm{Re}^{0.719}$
	Onduline and flat channel		$37.244\mathrm{Re}^{-0.243}$	$0.188\mathrm{Re}^{0.774}$
	Narrow-extended gap channel		$43.901\mathrm{Re}^{-0.228}$	$0.221\mathrm{Re}^{0.724}$

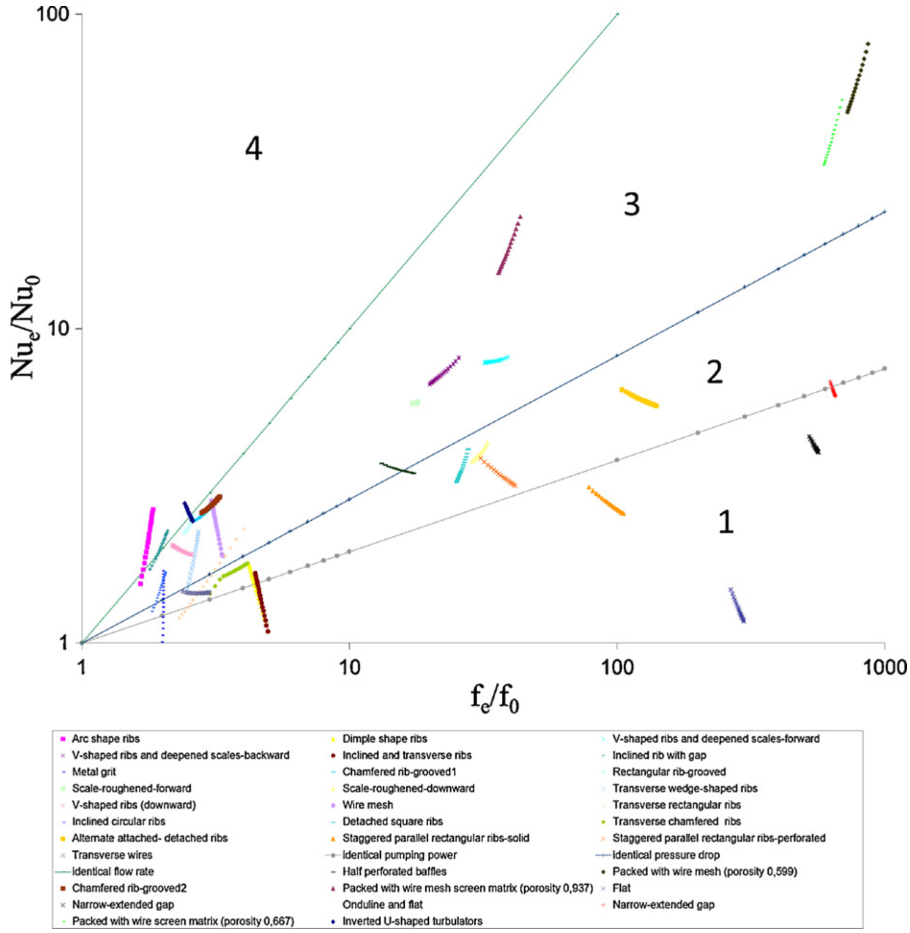


Fig. 7. Comparison of thermo-hydraulic performance of different heat transfer enhancement techniques in CHEs.

taken as the abscissa and ordinate, respectively. The coordinates are log–log based. From experimentally obtained data or numerically simulated results of such two ratios, a working point can be chosen in the plot. It is shown that the quadrant of the coordinate where both (Nu_e/Nu_0), (f_e/f_0) are greater than 1.0 can be divided by four regions corresponding to the different effectiveness of saving energy: Region 1 is characterized by enhanced heat transfer without energy-saving, where heat transfer enhancement is obtained with larger pressure drop penalty such that per identical pumping power the heat transfer is deteriorated; in Region 2 heat transfer is enhanced per identical pumping power but deteriorated per identical pressured drop, in Region 3 heat transfer is enhanced per identical pressure drop, and in Region 4 the heat transfer enhancement ratio is larger than the friction factor increase ratio under identical flow rate, which is the most favorable but also the most difficult region to reach for heat transfer enhancement study.

3.2.2. The discussion on best options

In Region 3, it is observed that the wire-screen mesh packing (Fig. 8) with the porosity of 0.599 has the highest heat transfer enhancement ratio. And with the increase of its porosity, the decrease in friction loss is found more than heat transfer enhancement, thus the packing with the porosity of 0.937 performs best. Under the identical pumping power constraint, the channel packed with wire mesh has the highest heat transfer enhancement ratio, and the same conclusion can be drawn under the identical pressure drop constraint.

Oriented for energy-saving purposes, it is the most ideal choice because the heat transfer enhancement ratio is larger than the friction factor increase ratio. For some fixed wire ribs shown in Fig. 9, like inverted U-shaped turbulators and inclined ribs with gap, penalty of friction is almost equal to the enhancement of heat transfer, especially for the arc shape ribs, enhancement of Nusselt number is slightly more than increase in friction factor. Under the identical flow rate constraint, arc shape ribs has the highest heat transfer enhancement ratio, followed by inverted U-shaped turbulators, inclined ribs with gap.

At the same time, from the plot we can find that the enhancement of heat transfer rate in the multi-pass flat channel (Fig. 10) is much less than the increase of power consumption, which means that from the energy-saving view point, the multi-pass flat channel design is the worst.

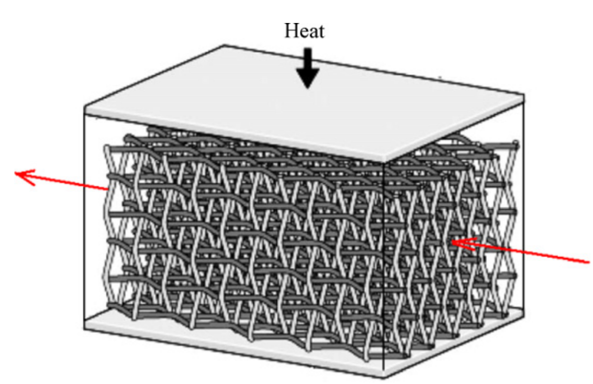
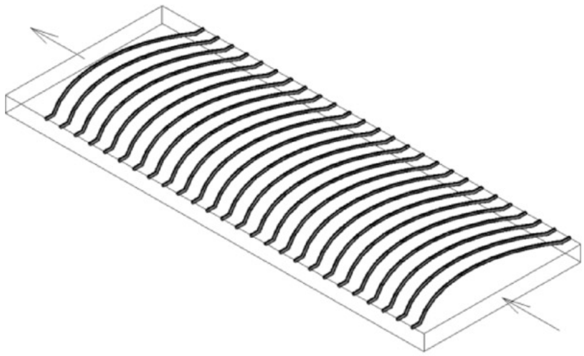
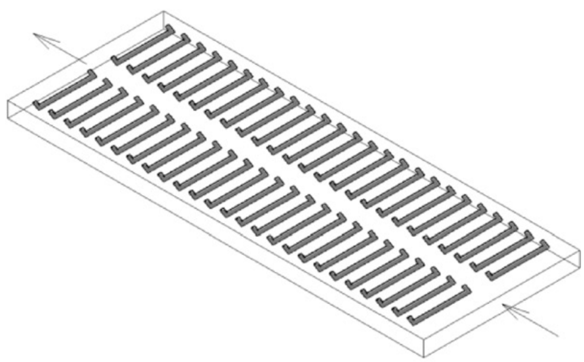


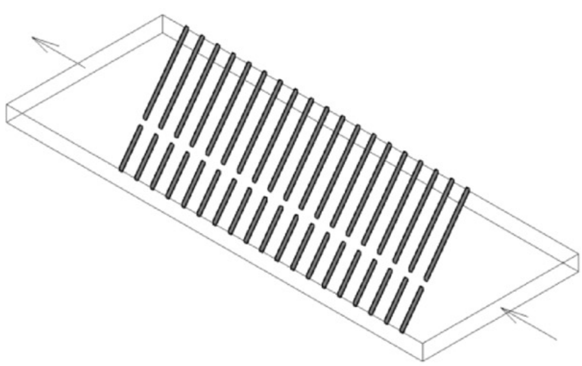
Fig. 8. Wire-screen mesh packing.



(a) Arc shaped rib



(b) Inverted U-shaped turbulator,



(c) Inclined rib with gap

Fig. 9. Fixed wire ribs.

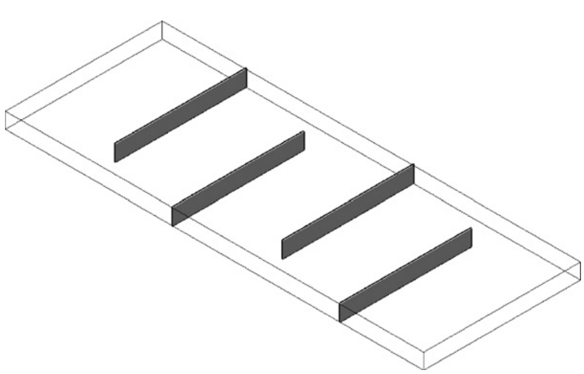


Fig. 10. Multi-pass flat channel.

Nevertheless, the heat transfer enhancement ratio and friction factor of every techniques are within a certain range. As a result, the most energy-saving technique should be selected under specific requirements.

4. Selection of CHE technologies for solar receiver application

A critical component of the Concentrated Solar Power (CSP) system is the solar receiver. This component will transfer heat to pressurized air that will generate electricity. The solar receiver will be operated at temperatures up to 900 °C and pressure in the range of 10 bar. There are major high temperature design, materials availability, and fabrication issues that need to be addressed.

Due to the high temperature requirements of the heat exchangers and the relatively high cost of the associated construction materials, CHEs are receiving attention for new generation of solar receiver system.

Firstly, the selection of CHE technologies depends on the operating conditions such as pressure, temperature. According to the review in Section 2 and comparison on the capabilities to cope with the operating conditions in Section 3.1, the designs meet the requirements for an application as the new generation of solar receiver include all-welded PHE (hybrid, Shell & Plate), PFHE, PCHE and ceramic heat exchanger designs. Among them, the diffusion bonded heat exchangers with micro-channels (diffusion bonded PFHE, PCHE) appear to be the more promising concept for high temperature application today. In spite of a more important pressure drop, this concept is best rated compared to the other concepts in particular in terms of reliability, mechanical resistance and compactness. The prospective materials are nickel-based alloy, in which Alloys 617 is ideal candidate for use at 900 °C.

Further selection is based on the results of comparison on the thermo-hydraulic performance in Section 3.2. The channel with wire-screen mesh packing has the highest heat transfer enhancement ratio under the identical pumping power and pressure drop constraint, which indicates that the heat exchanger with porous materials can offer the potential for a more effective solar receiver. Nowadays, the most promising porous materials are believed to be ceramic materials rather than metallic wire meshes in the past.

Both technologies, the diffusion bonded heat exchangers with micro-channels and ceramic heat exchanger, are future options for a high-performance solar receiver.

5. Conclusion

CHEs play an important role in saving and high-efficiency utilizing energy. In coming years, increasing demand for heat exchanger complying with the principles of ecological and economic sustainability will certainly further expand their industrial applications.

The major emphasis of this paper is placed on introducing the structures and heat transfer enhancement mechanisms of certain types of CHEs commonly used in industry or still studied in the laboratory (many specialized CHEs are not covered in this paper). Their development is summarized, as well as their major advantages and limitations. This broad overview of different types of CHEs will help the manufacturers to design and analyze for their specific needs.

Although a considerable database already exists for single-phase heat transfer in various types of CHEs, some of the data are not sufficient, incomplete and cannot be used primarily because of the difference in operating temperature conditions. Additional experimental work is needed on visualization and measurements of pressure drop, local velocity profiles and heat transfer coefficients to obtain more data, especially at high temperatures, in order to

validate CFD results and for the prediction of thermal–hydrodynamic behavior of CHEs.

The success of the new generation of solar receiver will depend in part on the correct selection of the CHE technologies. The demands of a high-temperature Brayton cycle challenge the boundaries of existing CHE technology for service in solar power systems.

Various heat transfer enhancement technologies in CHEs are compared on their capabilities to cope with given operating conditions and their thermo-hydraulic performance which is analyzed on the basis of available correlations of heat transfer and friction factor developed by various investigators quoted in the open literature. According to the results, a recommendation is made for the new generation of solar receiver. The proposed designs include diffusion bonded heat exchangers with micro-channels and ceramic heat exchanger.

This article serves as a starting point for further research in this important area. Among others in the review, that solar receivers based on CHE technology have been rarely reported, and therefore, extensive research work is required in this field for a comprehensive understanding to improve the uses of new energy sources and contribute to sustainability.

Acknowledgments

Authors thanks for their financial supports, the French-Chinese International Associated Laboratory on Sustainable Energy and the CNRS interdisciplinary programme on Energy (CNRS-PIE) via the SOLINTENSE project.

References

[1] Heller P, Pfänder M, Denk T, Tellez F, Valverde A, Fernandez J, et al. Test and evaluation of a solar powered gas turbine system. Solar Energy 2006;80:1225–30.
[2] Garcia P, Ferrière A, Flamant G, Costerg P, Soler R, Gagnepain B. Solar field efficiency and electricity generation estimations for a hybrid solar gas turbine project in France. ASME J Solar Energy Eng 2008;130/1:014502.
[3] Dostal V, Hejzlar P, Driscoll MJ. High-performance supercritical carbon dioxide cycle for next-generation nuclear reactor. Nucl Technol 2006;154:265–82.
[4] Shah RK. In: Kakac S, Bergles AE, Mayinger F, editors. Classification of heat exchangers, in heat exchangers: thermal–hydraulic fundamentals and design. Washington, DC: Hemisphere Publishing; 1981. p. 9–46.
[5] Mehendale SS, Jacobi AM, Shah RK. Fluid flow and heat transfer at micro- and meso-scales with application to heat exchanger design. Appl Mech Rev 1999;53(7):175–93.
[6] Shah RK, Sekulić DP. Fundamentals of heat exchanger design. New York: John Wiley & Sons; 2003. pp. 9–39.
[7] Shah RK. Compact heat exchanger technology and applications. In: Foumeny EA, Heggs PJ, editors. Heat exchanger engineering, vol. 2, compact heat exchangers: techniques for size reduction. London: Ellis Horwood; 1991. p. 1–29.
[8] Wang L, Sunden B, Manglik RM. Plate heat exchangers: design, applications and performance. Southampton, UK: WIT Press; 2007. pp. 8–45.
[9] Heggs PJ, Sandham P, Hallam RA, Walton C. Local transfer coefficients in corrugated plate heat exchangers channels, Trans IChemE, Part A. Chem Eng Res Des 1997;75(A7):641–5.
[10] Dovic D, Palm B, Svaic S. Generalized correlations for predicting heat transfer and pressure drop in plate heat exchanger channels of arbitrary geometry. Int J Heat Mass Trans 2009;52(19–20):4553–63.
[11] Elshafei EAM, Awad MM, El-Negiry E, Ali AG. Heat transfer and pressure drop in corrugated channels. Energy 2010;35(1):101–10.
[12] Focke WW, Knibbe PG. Flow visualization in parallel-plate ducts with corrugated walls. J Fluid Mech 1986;165:73–7.
[13] Herman CV, Mayinger F. Experimental investigation of the heat transfer in laminar forced convection flow in a grooved channel. In: Proc. of the 9th Int. Heat Transfer Conf. vol. 3, Jerusalem, Hetsroni G. Hemisphere, New York; 1990. p. 387–92.
[14] Herman CV, Mayinger F. Experimental analysis of forced convection heat transfer in a grooved channel. In: Sunden B, et al., editors. Proc. of the First Baltic heat transfer conference, Goeteborg, Sweden, August 26–28, In: Recent Advances in Heat Transfer, vol. 2. Amsterdam: Elsevier; 1992. p. 900–13.
[15] Mayinger F, Klas J. Compact heat exchangers. In: Heat transfer. (ICHEME symposium series no. 129). Institution of Chem. Engineers Ed., Rugby, UK, vol. 1. New York: Hemisphere; 1992. p. 35–46.
[16] Paras SV, Drosos EIP, Karabelas AJ, Chopard F. Counter-current gas/liquid flow through channels with corrugated walls-visual observations of liquid distribution and flooding, world conference on experimental heat transfer, fluid mechanics and thermodynamics, Thessaloniki, September 24–28; 2001.
[17] Kanaris AG, Mouza AA, Paras SV. Designing novel compact heat exchangers for improved efficiency using a CFD code. In: 1st Intern. Conference From scientific computing to computational engineering Athens, Greece; 2004.
[18] Sang I, Hyung N. Experimental study on flow and local heat/mass transfer characteristics inside corrugated duct. Int J Heat Fluid Flow 2006;27:21–32.
[19] Asano H, Takenaka N, Wakabayashi T, Fujii T. Visualization and void fraction distribution of downward gas–liquid two-phase flow in a plate heat exchanger by neutron radiography. In: Nuclear Instruments and Methods in Physics Research Section A: Accelerators, Spectrometers, Detectors and Associated Equipment, Volume 542, Issues 1–3, Proceedings of the Fifth International Topical Meeting on Neutron Radiography, 21; April 2005. pp. 154–60.
[20] Li XW, Meng JA, Li ZX. An experimental study of the flow and heat transfer between enhanced heat transfer plates for PHEs. Exp Therm Fluid Sci 2010;34(8):1194–204.
[21] Rao BP, Das SK. An experimental study on the influence of flow maldistribution on the pressure drop across a plate exchanger. J Fluids Eng, ASME Trans 2004;126:680–91.
[22] Rao BP, Sunden B, Das SK. An experimental investigation of the port maldistribution in small and large plate package exchangers. Appl Therm Eng 2006;26:1919–26.
[23] Durmus A, Benli H, Kurtbas I, Gul H. Investigation of heat transfer and pressure drop in plate heat exchangers having different surface profiles. Int J Heat Mass Trans 2009;52(5–6):1451–7.
[24] Jeong JY, Hong HK, Kim SK, Kang YT. Impact of plate design on the performance of welded type plate heat exchangers for sorption cycles. Int J Refrigerat 2009;32(4):705–11.
[25] Fernandes CS, Dias RP, Nóbrega JM, Afonso IM, Melo LF, Maia JM. Simulation of stirred yoghurt processing in plate heat exchangers. J Food Eng 2005;69:281–90.
[26] Fernandes CS, Dias RP, Nóbrega JM, Afonso IM, Melo LF, Maia JM. Thermal behaviour of stirred yoghurt during cooling in plate heat exchangers. J Food Eng 2006;76:433–9.
[27] Fernandes CS, Dias RP, Nóbrega JM, Maia JM. Laminar flow in chevron-type plate heat exchangers: CFD analysis of tortuosity, shape factor and friction factor. Chem Eng Proc 2007;46:825–33.
[28] Fernandes CS, Dias RP, Nóbrega JM, Maia JM. Friction factors of power-law fluids in chevron-type plate heat exchangers. J Food Eng 2008;89:441–7.
[29] Kanaris AG, Mouza AA, Paras SV. Flow and heat transfer in narrow channels with corrugated walls: a CFD code application. Chem Eng Res Des 2005;83(5):460–8.
[30] Kanaris AG, Mouza AA, Paras SV. Optimal design of a plate heat exchanger with undulated surfaces. Int J Therm Sci 2009;48(6):1184–95.
[31] Tsai YC, Liu FB, Shen PT. Investigations of the pressure drop and flow distribution in a chevron-type plate heat exchanger. Int Commun Heat Mass Trans 2009;36(6):574–8.
[32] Muley A, Manglik RM. Experimental study of turbulent flow heat transfer and pressure drop in a plate heat exchanger with Chevron plates. J Heat Trans 1999;121(1):110–7.
[33] Khan TS, Khan MS, Chyu MC, Ayub ZH. Experimental investigation of single phase convective heat transfer coefficient in a corrugated plate heat exchanger for multiple plate configurations. Appl Therm Eng 2010;30(8–9):1058–65.
[34] Selbaş R, Şencan A, Kılıç B. Alternative approach in thermal analysis of plate heat exchanger. Heat Mass Trans 2009;45:323–9.
[35] Ayub ZH. Plate heat exchanger literature survey and new heat transfer and pressure drop correlations for refrigerant evaporators. Heat Trans Eng 2003;24(5):3–16.
[36] Focke WW, Zachariades J, Oliver I. The effect of the corrugation inclination angle on the thermo hydraulic performance of plate heat exchangers. Int J Heat Mass Trans 1985;28(8):1469–79.
[37] Wang L, Sundén B, Richardson P. Optimizing plate heat exchanger design and operation. In: Richardson PS, editor. Improving the thermal processing of foods. Boca Raton, Florida, USA: CRC Press; 2004 p. 205.
[38] Lee S, Speight JG, Loyalka SK. Handbook of alternative fuel technologies. New York: Taylor & Francis; 2007.
[39] Dahlgren A, Kallrot M, Stromblad M, inventors. Plate heat exchanger, June 14. Patent WO/1986/006463; 1985.
[40] Hesselgreaves JE. Compact heat exchangers: selection, design and operation. Amsterdam: Pergamon; 2001.
[41] Davison Roger C, Mathur Achint P, inventors; Tranter, Inc., assignee. All-welded plate heat exchanger, June 14. US Patent 5469914; 1993.
[42] Mathur Achint P, Fulmer Jason M, inventors; Delaware Capital Formation, Inc., assignee. Shell and plate heat exchanger, January 10. US Patent 7004237; 2002.
[43] Mathur Achint P, Fulmer Jason M, inventors. Shell and plate heat exchanger, January 10. US Patent 20030000688; 2002.
[44] Jullien C, Couillard Y, inventors; Packinox SA., assignee. Heat exchanger of the plate type, October 20. US Patent 5333681; 1992.
[45] Würfel N, Ostrowski R. Experimental investigations of heat transfer and pressure drop during the condensation process within plate heat exchangers of the herringbone-type. Int J Therm Sci 2004;43:59–68.
[46] Bojesen C, inventors. Heat exchanger plate, July 12. Patent WO2008071356; 2007.

[47] Rausing H, inventors; Eco Lean Research & Development A/S, assignee. Heat exchanger plate and plate heat exchanger comprising such plates, November 19. US Patent 20070144711; 2004.
[48] Luan ZJ, Zhang GM. Flow resistance and heat transfer characteristics of a new type of heat exchanger. J Hydrodyn 2008;20(4).
[49] Guo ZY, Li DY, Wang BX. A novel concept for convective heat transfer enhancement. Int J Heat Mass Trans 1998;41(14):2221–5.
[50] Guo ZY, Tao WQ, Shah RK. The field synergy (coordination) principle and its applications in enhancing single phase convective heat transfer. Int J Heat Mass Trans 2005;48(9):1797–807.
[51] Thonon B, Breuil E, 2001. Compact heat exchangers technologies for HTRs recuperator application. In: Proceedings of the technical committee meeting on gas turbine power conversion systems for modular HTGRs-Palo Alto, California, IAEA-TECDOC, November 14–16; 2000, p. 1–11.
[52] Lozano A, Barreras F, Fueyo N, Santodomingo S. The flow in an oil/water plate heat exchanger for the automotive industry. Appl Therm Eng 2008;28(10):1109–17.
[53] Katzel J. Heat exchanger basics (A Plant Engineering Exclusive), Plant Engineering, April 1; 2000.
[54] Sherman SR, Chen Y. Heat exchanger testing requirements and facility needs for the NHI/NGNP project, WSRC-STI-2008-00152, April; 2008.
[55] The standards of the brazed aluminium plate-fin heat exchanger manufacturers' association, 2nd edition, ALPEMA; 2000.
[56] Zhang LW, Balachandar S, Tafti DK, Najjar FM. Heat transfer enhancement mechanisms in inline and staggered parallel-plate fin heat exchangers. Int J Heat Mass Trans 1997;40(10):2307–25.
[57] Jacobi AM, Shah RK. Heat transfer surface enhancements through the use of longitudinal vortices: a review of recent progress. Exp Therm Fluid Sci 1995;11:295–309.
[58] Valencia A, Fiebig M, Mitra NK. Heat transfer enhancement by longitudinal vortices in a fin-tube heat exchanger element with flat tubes. J Heat Transer 1996;118:209–11.
[59] Mittal R, Balachandar S. Effect of three-dimensionality on the lift and drag of nominally two-dimensional cylinders. Phys Fluids 1995;7: 1841–65.
[60] Brockmeier U, Guentermann T, Fiebig M. Performance evaluation of a vortex generator heat transfer surface and comparison with different high performance surfaces. Int J Heat Mass Trans 1993;36:2575–87.
[61] Sheik Ismail L, Velraj R, Ranganayakulu C. Studies on pumping power in terms of pressure drop and heat transfer characteristics of compact plate-fin heat exchangers—a review. Renew Sustain Energy Rev 2010;14(1): 478–85.
[62] Hao Peng, Xiang Ling. Neural networks analysis of thermal characteristics on plate-fin heat exchangers with limited experimental data. Appl Therm Eng 2009;29(11–12):2251–6.
[63] Sachdeva G, Kasana KS, Vasudevan R. Analysis on heat transfer enhancement by using triangular shaped inserts as secondary fins in cross flow plate fin heat exchanger. Int J Dyn Fluids 2010;6(1):41–7.
[64] Sachdeva G, Vasudevan R, Kasana KS. Computation of heat transfer enhancement in a plate-fin heat exchanger with triangular inserts and delta wing vortex generator. Int J Numer Meth Fluids 2009.
[65] Adderley Colin I, Fowler John O, Wignall Michael F, inventors; Rolls-Royce And Associates Limited, Rolls-Royce plc., assignee. Heat exchanger, November 12. US Patent 5573060; 1996.
[66] Dudfield CD, Chen R, Adcock PL. A carbon monoxide PROX reactor for PEM fuel cell automotive application. Int J Hydrogen Energy 2001;26(7): 763–75.
[67] Reay D. Learning from experiences with compact heat exchangers, Center for the Analysis and Dissemination of Demonstrated Energy Technologies (CADDET), Series No. 25, Netherlands; 1999.
[68] Ferrato M, Thonon B. A compact ceramic plate-fin heat exchanger for gas turbine heat recovery. In: Shah RK, editor. Compact heat exchanger for the process industry. Begell House Inc.; 1997.
[69] Fan Y, Luo L. Recent applications of advances in microchannel heat exchangers and multi-scale design optimization. Heat Trans Eng 2008;29:461–74.
[70] Dewson SJ. The development of high efficiency heat exchangers for helium gas cooled reactors, Report # 3213, International Conference on Advanced Nuclear Power Plants (ICAP), Cordoba, Spain; 2003.
[71] Kim DE, Kim MH, Cha JE, Kim SO. Numerical study for heat transfer and pressure drop of supercritical carbon dioxide fluid with channel bending angle in Printed Circuit Heat Exchanger, Korean Society of Mechanical Engineering (KSME) 2008, Division of Thermal Engineering; 2008.
[72] Pra F, Tochon P, Mauget C, Fokkens J, Willemsen S. Promising designs of compact heat exchangers for modular HTRs using the Brayton cycle. Nucl Eng Des 2008;238(11):3160–73.
[73] Gschwind, Regele A, Kottke V. Sinusoidal wavy channels with Taylor–Görtler vortices. Exp Therm Fluid Sci 1995;11:270–5.
[74] Sabharwall P. Engineering design elements of a two-phase thermosyphon to transfer NGNP thermal energy to a hydrogen plant, INL/EXT-09-15383; 2009.
[75] Tsuzuki N, Kato Y, Ishiduka T. High performance printed circuit heat exchanger. Appl Therm Eng 2007;27(10):1702–7.
[76] Haynes BS. High-effectiveness micro-exchanger performance. AIChE 2002 Spring National Meeting, New Orleans; 2002.
[77] Pieve M. A calculation method for the optimized thermal-fluid dynamic sizing of heat exchangers. Heat Trans Eng 2008;29(6):556–64.
[78] Southall D, Renaud Le P, Stephen JD. Design considerations for compact heat exchangers. In: Proceedings of ICAPP '08 Anaheim, CA USA, June 8–12; 2008.
[79] Ngo TL, Kato Y, Nikitin K, Ishizuka T. Heat transfer and pressure drop correlations of micro-channel heat exchangers with S-shaped and zigzag fins for carbon dioxide cycles. Exp Therm Fluid Sci 2007;32:560–70.
[80] Ngo TL, Kato Y, Nikitin K, Tsuzuki N. New printed circuit heat exchanger with S-shaped fins for hot water supplier. Exp Therm Fluid Sci 2006;30: 811–9.
[81] Kim DE, Kim MH, Cha JE, Kim SO. Numerical investigation on thermal–hydraulic performance of new printed circuit heat exchanger model. Nucl Eng Des 2008;238:3269–76.
[82] Reay D. The role of process intensification in cutting greenhouse gas emissions. Appl Therm Eng 2008;28(16) [Selected Papers from the 10th Conference on Process Integration,Modelling and Optimisation for Energy Saving and Pollution Reduction, p. 2011–9].
[83] Reay DA. Compact heat exchangers, enhancement and heat pumps. Int J Refrigerat 2002;25(4):460–70.
[84] Sabharwall P, Gunnerson F, Tokuhiro A, Utgikar V, Weaver K, Sherman S. Theoretical design of a thermosyphon for a process heat removal from Next Generation Nuclear Plant (NGNP) for production of hydrogen, INL/EXT-07-13433, Department of Energy (ii); 2007.
[85] Mellouli S, Askri F, Dhaou H, Jemni A, Ben Nasrallah S. A novel design of a heat exchanger for a metal-hydrogen reactor. Int J Hydrogen Energy, 32(15), International Symposium on Solar-Hydrogen-Fuel Cells; 2007. p. 3501–7.
[86] Picon-Nunez M, Canizalez-Davalos L, Martinez-Rodriguez G, Polley GT. Shortcut design approach for spiral heat exchangers. Food Bioproducts Process 2007;85(4):322–7.
[87] Shih HY, Huang YC. Thermal design and model analysis of the Swiss-roll recuperator for an innovative micro gas turbine. Appl Therm Eng 2009;29(8–9):1493–9.
[88] Shih HY, Wang D, Kuo CR. Feasibility study of an innovative micro gas turbine with a Swiss-roll recuperator. In: Proceedings of ASME Turbo Expo v5 part A; 2006. p. 459–66.
[89] Kuo CR, Wang TW, Wu JR, Shih HY, Hsiung TP, Chang CY, inventors; Industrial Technology Research Institute, assignee. Gas turbine engine, March 30. US Patent 6711889 B2; 2004.
[90] Gueguen JM, inventors; Spirec (Societe Anonyme), assignee. Spiral heat exchangers, April 05. US Patent 6874571; 2005.
[91] Mc Donald C. Low-cost compact primary surface recuperator concept for microturbines. Appled Therm Eng 2000;20:471–97.
[92] Kuo CH, Ronney PD. Numerical modeling of non-adiabatic heat-recirculating combustors. Proc Combust Inst 2007;31(2):3277–84.
[93] ASTM Standard C242-01, 2007, Standard Terminology of Ceramic Whitewares and Related Products," ASTM International, West Conshohocken, PA. doi:10.1520/C0242-01R07, www.astm.org; 2007.
[94] Sommers A, Wang Q, Han X, T'Joen C, Park Y, Jacobi A. Ceramics and ceramic matrix composites for heat exchangers in advanced thermal systems—a review. Appl Therm Eng 2010;30(11–12):1277–91.
[95] Rohde M, Südmeyer I, Urbanek A, Torge M. Joining of alumina and steel by a laser supported brazing process. Ceram Int 2009;35:333–7.
[96] Lippmann W, Knorr J, Wolf R, Rasper R, Exner H, Reinecke A-M, et al. Laser joining of silicon carbide—a new technology for ultra-high temperature resistant joints. Nucl Eng Des 2004;231:151–61.
[97] Snead LL, Katoh Y, Kohyama A, Bailey JL, Vaughn NL, Lowden RA. Evaluation of neutron irradiated near-stoichiometric silicon carbide fiber composites, Journal of Nuclear Materials, Volumes 283–7, Part 1, 9th Int. Conf. on Fusion Reactor Materials, December; 2000. p. 551–5.
[98] Greil P, Lifka T, Kaindl A. Biomorphic cellular silicon carbide ceramics from wood: II. Mechanical properties. J Eur Ceram Soc 1998;18(14):1975–83.
[99] Steen M, Ranzani L. Potential of SiC as a heat exchanger material in combined cycle plant. Ceram Int 2000;26(8):849–54.
[100] Amirthan G, Udaya kumar A, Balasubramanian M. Thermal conductivity studies on Si/SiC ceramic composites. Ceram Int 2011;37(1):423–6.
[101] Alm B, Imke U, Knitter R, Schygulla U, Zimmermann S. Testing and simulation of ceramic micro heat exchangers, Chemical Engineering Journal, 135, Supplement 1, Microreaction Technology IMRET 9: Proceedings of the Ninth International Conference on Microreaction Technology—IMRET9 Special Issue, 15 January; 2008. p. S179–S184.
[102] Schulte-Fischedick J, Drei[ss]igacker V, Tamme R. An innovative ceramic high temperature plate-fin heat exchanger for EFCC processes. Appl Therm Eng 2007;27(8–9):1285–94.
[103] Islamoglu Y. Numerical analysis of the influence of a circular fin with different profiles on the thermal characteristics in a ceramic tube of heat transfer equipment. Int J Pressure Vessels Piping 2004;81(7):583–7.
[104] Islamoglu Y. Finite element model for thermal analysis of ceramic heat exchanger tube under axial non-uniform convective heat transfer coefficient. Mater Des 2004;25(6):479–82.
[105] Fend T, Hoffschmidt B, Pitz-Paal R, Reutter O, Rietbrock P. Porous materials as open volumetric solar receivers: experimental determination of thermophysical and heat transfer properties. Energy 29;5–6: 823–33 [SolarPACES 2002; April–May 2004].
[106] Fend T, Pitz-Paal R, Reutter O, Bauer J, Hoffschmidt B. Two novel high-porosity materials as volumetric receivers for concentrated solar radiation. Solar Energy Mater Solar Cells 2004;84(1–4):291–304 [International Solar Energy Society World Congress 2003, October].

[107] McDonald CF. Recuperator considerations for future higher efficiency microturbines. Appl Therm Eng 2003;23(January (12)):1463–87.
[108] Fan JF, Ding WK, Zhang JF, He YL, Tao WQ. A performance evaluation plot of enhanced heat transfer techniques oriented for energy-saving. Int J Heat Mass Trans 2009;52(1–2):33–4.
[109] Prasad BN, Saini JS. Effect of artificial roughness on heat transfer and friction factor in a solar air heater. Solar Energy 1988;41(6):555–60.
[110] Hwang JJ, Liou TM. Heat transfer in a rectangular channel with perforated turbulence promoters using holographic interferometry measurement. Int J Heat Mass Trans 1995;38(17):3197–207.
[111] Liou TM, Wang WB. Laser holographic interferometry study of developing heat transfer in a duct with a detached rib array. Int J Heat Mass Trans 1995;38(1):91–100.
[112] Gupta D, Solanki SC, Saini JS. Thermohydraulic performance of solar air heaters with roughened absorber plates. Solar Energy 1997;61(1):33–42.
[113] Leung CW, Kang HJ, Probert SD. Horizontal simulated printed-circuit board assembly in fully-developed laminar-flow convection. Appl Energy 1997;56(1):71–91.
[114] Saini RP, Saini JS. Heat transfer and friction factor correlations for artificially roughened ducts with expanded metal mesh as roughened element. Int J Heat Mass Trans 1997;40(4):973–86.
[115] Tsia JP, Hwang JJ. Measurements of heat transfer and fluid flow in a rectangular duct with alternate attached-detached rib-arrays. Int J Heat Mass Trans 1999;42(11):2071–83.
[116] Karwa R, Solanki SC, Saini JS. Heat transfer coefficient and friction factor correlations for the transitional flow regime in rib-roughened rectangular ducts. Int J Heat Mass Trans 1999;42(9):1597–615.
[117] Verma SK, Prasad BN. Investigation for the optimal thermohydraulic performance of artificially roughened solar air heaters. Renew Energy 2000;20(1):19–36.
[118] Momin AME, Saini JS, Solanki SC. Heat transfer and friction in solar air heater duct with V-shaped rib roughness on absorber plate. Int J Heat Mass Trans 2002;45(16):3383–96.
[119] Bhagoria JL, Saini JS, Solanki SC. Heat transfer coefficient and friction factor correlations for rectangular solar air heater duct having transverse wedge shaped rib roughness on the absorber plate. Renew Energy 2002;25(3):341–69.
[120] Chandra PR, Alexander CR, Han JC. Heat transfer and friction behaviors in rectangular channels with varying number of ribbed walls. Int J Heat Mass Trans 2003;46(3):481–95.
[121] Chang SW, Liou TM, Lu MH. Heat transfer of rectangular narrow channel with two opposite scale-roughened walls. Int J Heat Mass Trans 2005;48(19–20):3921–31.
[122] Jaurker AR, Saini JS, Gandhi BK. Heat transfer and friction characteristics of rectangular solar air heater duct using rib-grooved artificial roughness. Solar Energy 2006;80(8):895–907.
[123] Layek A, Saini JS, Solanki SC. Second law optimization of a solar air heater having chamfered rib–groove roughness on absorber plate. Renew Energy 2007;32(12):1967–80.
[124] Layek A, Saini JS, Solanki SC. Heat transfer and friction characteristics for artificially roughened ducts with compound turbulators. Int J Heat Mass Trans 2007;50(23–24):4845–54.
[125] Karmare SV, Tikekar AN. Heat transfer and friction factor correlation for artificially roughened duct with metal grit ribs. Int J Heat Mass Trans 2007;50(21–22):4342–51.
[126] Aharwal KR, Gandhi BK, Saini JS. Experimental investigation on heat-transfer enhancement due to a gap in an inclined continuous rib arrangement in a rectangular duct of solar air heater. Renew Energy 2008;33(4):585–96.
[127] Varun, Saini RP, Singal SK. Investigation of thermal performance of solar air heater having roughness elements as a combination of inclined and transverse ribs on the absorber plate. Renew Energy 2008;33(6):1398–405.
[128] Chang SW, Liou T-M, Chiang KF, Hong GF. Heat transfer and pressure drop in rectangular channel with compound roughness of V-shaped ribs and deepened scales. Int J Heat Mass Trans 2008;51(3–4):457–68.
[129] Saini RP, Verma Jitendra. Heat transfer and friction factor correlations for a duct having dimple-shape artificial roughness for solar air heaters. Energy 2008;33(8):1277–87.
[130] Saini SK, Saini RP. Development of correlations for Nusselt number and friction factor for solar air heater with roughened duct having arc-shaped wire as artificial roughness. Solar Energy 2008;82(12):1118–30.
[131] Bopche SB, Tandale MS. Experimental investigations on heat transfer and frictional characteristics of a turbulator roughened solar air heater duct. Int J Heat Mass Trans 2009;52(11–12):2834–48.
[132] Karwa Rajendra, Maheshwari BK. Heat transfer and friction in an asymmetrically heated rectangular duct with half and fully perforated baffles at different pitches. Int Commun Heat Mass Trans 2009;36(3):264–8.
[133] Prasad SB, Saini JS, Singh KM. Investigation of heat transfer and friction characteristics of packed bed solar air heater using wire mesh as packing material. Solar Energy 2009;83(5):773–83.
[134] Varshney L, Saini JS. Heat transfer and friction factor correlations for rectangular solar air heater duct packed with wire mesh screen matrices. Solar Energy 1998;62(4):255–62.
[135] Thakur NS, Saini JS, Solanki SC. Heat transfer and friction factor correlations for packed bed solar air heater for a low porosity system. Solar Energy 2003;74(4):319–29.
[136] Kurtbas I, Durmus A. Efficiency and exergy analysis of a new solar air heater. Renew Energy 2004;29(9):1489–501.